CMI

Check for updates

ARTICLE

ADAP restraint of STAT1 signaling regulates macrophage phagocytosis in immune thrombocytopenia

Yiwei Xiong [1], Yanli Li[1], Xinxing Cui[1], Lifeng Zhang[2], Xiaodong Yang[3] and Hebin Liu[1,4 ✉]

Heightened platelet phagocytosis by macrophages accompanied by an increase in IFN-γ play key roles in the etiology of immune thrombocytopenia (ITP); however, it remains elusive how macrophage-mediated platelet clearance is regulated in ITP. Here, we report that adhesion and degranulation-protein adaptor protein (ADAP) restrains platelet phagocytosis by macrophages in ITP via modulation of signal transducer and activator of transcription 1 (STAT1)-FcγR signaling. We show that ITP was associated with the underexpression of ADAP in splenic macrophages. Furthermore, macrophages from $Adap^{-/-}$ mice exhibited elevated platelet phagocytosis and upregulated proinflammatory signaling, and thrombocytopenia in $Adap^{-/-}$ mice was mitigated by the depletion of macrophages. Mechanistically, ADAP interacted and competed with STAT1 binding to importin α5. ADAP deficiency potentiated STAT1 nuclear entry, leading to a selective enhancement of FcγRI/IV transcription in macrophages. Moreover, pharmacological inhibition of STAT1 or disruption of the STAT1-importin α5 interaction relieved thrombocytopenia in $Adap^{-/-}$ mice. Thus, our findings not only reveal a critical role for ADAP as an intracellular immune checkpoint for shaping macrophage phagocytosis in ITP but also identify the ADAP-STAT1-importin α5 module as a promising therapeutic target in the treatment of ITP.

Keywords: ADAP; Immune thrombocytopenia; Fc gamma receptor; Platelet phagocytosis; STAT1

INTRODUCTION

Immune thrombocytopenia (ITP) is an acquired autoimmune disorder characterized by low platelet counts with an increased risk of bleeding complications [1, 2], which occurs with an annual incidence of approximately 2 to 6 per 100,000 children and 3 per 100,000 adults [3]. ITP is also secondary to many other diseases, including autoimmune diseases such as systemic lupus erythematosus, cancers and viral infections such as hepatitis C virus, human immunodeficiency virus and severe acute respiratory syndrome coronavirus 2 (SARS-CoV-2) infections [2, 4–6].

In approximately 70% of all ITP patients, autoantibodies are detected, predominantly against platelet glycoproteins GPIIb/IIIa and GPIb/IX [4, 7]. Excessive destruction of autoantibody-opsonized platelets by Fcγ receptor (FcγR)-bearing phagocytes is central to the immune pathophysiology of ITP [8–10]. FcγRs are immunoglobulin G (IgG)-specific transmembrane receptor molecules expressed on the surface of myeloid cells, and the FcγR family mainly consists of several activating receptors, including FcγRI (human and mouse), FcγRIIA and IIC (human), FcγRIIIA (human), FcγRIII (mouse) and FcγRIV (mouse), and one inhibitory receptor, FcγRIIB. While FcγRI is the high-affinity receptor for IgG subclasses in both humans and mice, FcγRIV also binds to IgG2a and 2b with high affinity in mice [11, 12]. Of note, the expression of FcγRI and the ratio of FcγRIIA/FcγRIIB on monocytes were significantly increased in some ITP patients [13]. FcγRI and FcγRIII,

but not FcγRIIA, are responsible for the ITP splenic macrophage phagocytosis of GPIIb/IIIa autoantibody-opsonized platelets [10]. In addition to the phagocytes, abnormal CD8^{+} T cells-mediated cytotoxicity also contributes to the platelet destruction in ITP [8, 14, 15].

ITP is often accompanied by a progressive increase in IFN-γ [16, 17]. Signal transducer and activator of transcription 1 (STAT1) is the key mediator of IFN-γ signaling [18]. Upon activation by the IFN-γ-Janus kinase signaling axis, STAT1 is phosphorylated at Tyr-701 (Y701). The activated pY701-STAT1 assembles into a homodimer and is then translocated into the nucleus to transactivate IFN-stimulated genes [19]. Notably, efficient nuclear import of activated STAT1 requires the recognition and binding of the noncanonical nuclear localization sequence (NLS) of STAT1 by importin α5, a nuclear transport receptor [20, 21]. Interestingly, heterozygous STAT1 gain-of-function mutations have been increasingly identified in ITP patients, whereas the functions of these mutations underlying the etiology of ITP remain unknown [22, 23].

Adhesion and degranulation-protein adaptor protein (ADAP, also known as FYB), first identified as an adaptor protein in T cells, has been implicated in the maintenance of platelet homeostasis. ADAP-knockout mice display mild thrombocytopenia with defects in platelet activation and biogenesis [24–27]. Moreover, two parallel studies converge on linking the pathogenic variants or

mutations of the ADAP gene with recessive thrombocytopenia in humans [28, 29]. Despite these findings, the functional role of ADAP in macrophage-mediated platelet clearance in the etiology of thrombocytopenia remains elusive. Here, we report that ADAP underexpression in splenic tissue is associated with thrombocytopenia, which can be reversed by macrophage depletion. ADAP constrains FcγR-mediated platelet phagocytosis by targeting the STAT1-importin α5 complex. Pharmacological inhibition of STAT1 or disruption of the STAT1-importin α5 interaction mitigate the thrombocytopenia in $Adap^{-/-}$ mice. Together, our data illustrate the ADAP-STAT1 module as a key regulatory component for platelet phagocytosis by macrophages and thus provide a potential therapeutic target for ITP.

MATERIALS AND METHODS

Clinical specimens
Spleen tissues were collected from 10 patients with ITP who underwent splenectomy (3 females and 7 males, age range 13–71 years, median platelet counts 37.5×10^9/L) and 15 non-ITP patients with splenic trauma (5 females and 10 males, age range 17–72 years, median platelet counts 207×10^9/L). Formalin-fixed and paraffin-embedded tissue slides were prepared using the same standardization procedure. Peripheral blood mononuclear cells (PBMCs) were isolated from heparinized blood provided by 5 patients with ITP (3 females and 2 males, age range 25–71 years, median platelet counts 29×10^9/L). Patient characteristics were given in Suppl. Table 1. This study was approved by the Institutional Review Board of the Dushu Lake Hospital Affiliated to Soochow University and conducted in compliance with the Declaration of Helsinki. Written informed consent for the use of samples was acquired from all patients.

Animals
$Adap^{-/-}$ and $Skap1^{-/-}$ mice were kind gifts from Dr. CE Rudd (University of Cambridge, UK), which were originally generated by Peterson et al. [25] and Wang et al. [30] respectively. WT C57BL/6 J obtained from GemPharmatech were used as controls for KO animals. The protein levels of ADAP in $Adap^{-/-}$ and WT C57BL/6 J mice were verified in Suppl. Fig. 1A. All mice were housed in specific pathogen-free facilities at Soochow University. All animal studies were approved by the Animal Ethics Committee of Soochow University. Age- and sex-matched mice between 6 and 8 weeks were used.

To deplete macrophages in vivo, mice were treated with 5 mg/ml liposomal clodronate or PBS-liposomes at a dose of 10 ml/kg via intravenous injection (i.v.). CD4+, CD8+ T cells, and B cells were depleted by treatment with 500 μg/kg of anti-CD4, anti-CD8a, or anti-CD20 in saline via intraperitoneal injection (i.p.) on days 0, 1, 3. Control mice received the same dose of isotype control antibody in saline. Daily doses of fludarabine (50 mg/kg) and ivermectin (1 or 3 mg/kg) were given to mice by i.v. and i.p., respectively.

Antibodies and reagents
Antibodies used were listed in Suppl. Table 2. Fludarabine monophosphate (TCI Chemicals) and ivermectin (MedChemExpress) were freshly prepared by dissolving in DMSO at high concentrations and further diluted in saline (5% DMSO) for injection. Clodronate liposomes and PBS liposomes were obtained from Yeasen. Recombinant IFN-γ was purchased from PeproTech. Aggregated IgG (AIgG) was prepared by heating mouse serum IgG (Sigma) at 62 °C for 30 min and centrifuging at $18000 \times g$ for 20 min.

Primary cells and cell lines
Bone marrow-derived macrophages (BMDMs) were obtained by flushing the bone marrow of femurs and tibias from mice and cultured in RPMI 1640 medium supplemented with 10% fetal bovine serum, 20% L929-conditioned medium, 100 U/ml penicillin/streptomycin, 2 mM L-glutamine, and 50 μM β-mercaptoethanol for 6 days. Mouse splenic macrophages were prepared from dispersed splenocytes and cultured in medium as described for BMDMs without L929-conditioned medium as previously described [31]. Immortalized BMDMs were prepared as previously described [32]. Monocytes were purified from patient PBMCs by CD14 positive selection using human CD14 microbeads (Miltenyi Biotec, Germany). Monocyte-derived macrophages were prepared as previously described [33]. RAW 264.7 and HEK 293 T cells were purchased from ATCC

and maintained in DMEM supplemented with 10% FBS and 100 U/ml penicillin/streptomycin.

Platelet counting
Blood was collected via submandibular bleeding and diluted in acid citrate dextrose (ACD) buffer (39 mM citric acid, 75 mM sodium citrate, 135 mM dextrose, pH 7.4). For the enumeration of reticulated platelets, fresh blood dilution as described above was incubated with 10 μg/ml thiazole orange (Sigma) in the dark for 30 min. Platelets were enumerated in a flow rate-calibrated FACSCalibur or Celesta flow cytometer (Becton Dickinson) as previously described [34]. Each sample was incubated with FITC-conjugated anti-CD41 to ensure the gating of the platelet population.

In vivo platelet clearance assay
Platelets were labelled with 8 μM DilC18(3) (Dil) for 60 min, followed by opsonization with 2 μg/ml R300 for another 60 min, and were transfused to recipients through tail vein (1×10^8 platelets/mice). Mice were bled at 1 min, 5 min, 10 min, 15 min, and 30 min. The fractions of labelled platelet remaining in the circulation were determined by flow cytometry.

In vitro phagocytosis assay
For the IgG-opsonized platelet phagocytosis assay, platelets were prepared from whole blood in ACD buffer by centrifugation and adjusted to 10^9/ml in the presence of 5 μM prostaglandin E1 (Sigma). Platelets were incubated with 8 μM Dil for 30 min followed by opsonization with 5 μg β3-integrin monoclonal antibody (anti-ITGB3/CD61, rabbit IgG) for another 30 min. Opsonized platelets were washed and incubated with peritoneal macrophages at 37 °C for the indicated times. Macrophages were washed extensively with PBS and detached using 10 mM EDTA at 4 °C. Extracellular fluorescence was quenched by 0.1% Trypan Blue. For the IgG-opsonized SRBC phagocytosis assay, fresh sheep red blood cells (SRBCs, Hongquan Biotech. Inc.) were labeled with PKH26 (Sigma–Aldrich) according to the manufacturer's instructions and opsonized with a subagglutinating concentration of rabbit anti-SRBC antibody (polyclonal IgG, Rockland) at 37 °C for 30 min. The opsonized SRBCs were then added to macrophages at an SRBC/macrophage ratio of 20:1 and incubated at 37 °C for the indicated times. Unbound SRBC was removed by hypotonic lysis with ACK buffer for 1 min at room temperature. For the phagocytosis of complement-opsonized zymosan particles, mouse serum-opsonized Alexa Fluor 488-conjugated zymosan A bioparticles [35] were added to macrophages and incubated at 37 °C for the indicated time. Cells were fixed in 4% paraformaldehyde and subjected to flow cytometric analysis. The phagocytic index was calculated as the mean fluorescence intensity multiplied by the frequency of Dil-, PKH26- or Alexa Fluor 488-positive cells [36].

Measurement of oxidative burst
BMDMs were rinsed with PBS, lifted from culture dishes, resuspended at 2.5×10^5 cell/ml in prewarmed Krebs-Ringer phosphate buffer (125 mM NaCl, 8 mM Na_2HPO_4, 2 mM NaH_2PO_4, 5 mM KCl, 5 mM glucose, 1 mM $CaCl_2$, 1.5 mM $MgCl_2$), and collected by flow cytometry to determine the baseline fluorescence for 1 min before stimulation with FcOxyBURST Green reagent at a concentration of 120 μg/ml at 37 °C. Changes in green fluorescence over a 10-min period were monitored using a FACSCalibur flow cytometer as described previously [37].

Flow cytometry
A single cell suspension was prepared from spleens by sieving and pipetting, followed by ACK lysis for 3 min and washing with FACS buffer (2% FCS, 2 mM EDTA in PBS). Cells were then stained with the antibodies for 30 min and fixed in 2% paraformaldehyde. Data were acquired on a FACSCalibur or Celesta flow cytometer, and data were analyzed using FlowJo software (TreeStar).

Plasmids, lentiviral transduction and luciferase reporter assay
HA tagged-ADAP has been described previously [38]. Human STAT1 cDNA was subcloned into the pcDNA3.1 + /C-(K)-DYK expression vector (Genscript). GFP-tagged KPNA1/importin α5 was purchased from Sino Biological. ADAP and STAT1 mutants were generated by a site-directed mutagenesis kit (Yeasen). Fcgr1-LUC was constructed by inserting fragments from the Fcgr1 promoter (from −189 to +1), which contains a

STAT1-binding site [39], into the pTA-LUC firefly luciferase plasmid (Clontech). Fcgr4-LUC was constructed by inserting fragments from the Fcgr4 promoter (from −1000 to +1) into the pTA-LUC plasmid. The guide RNA sequences targeting *Adap* and *Kpna1* were designed using the GPP sgRNA Designer [40] and cloned into a CRISPR–Cas9-based lentiviral vector (plentiCRISPRv2, Addgene, 52962) as described in [41]. Cloned oligonucleotides were as follows: sgRNA-*Adap*: 5′-TAGGTAGGTTTCGCTGCCAA-3′; sgRNA-*Kpna1*: 5′-CAAGAAAGGACATTCAGACA-3′. Scramble sgRNA (5′-GCACTACCAGAGCTAACTCA-3′) [42] was cloned and used in parallel as a negative control. shRNAs targeting ADAP (#1, 5′- GCAAAGGCCA GACGTCTTA-3′; #2, 5′-GAGATGAAGTTTACGATGAT-3′) and control shRNA targeting EGFP were described previously [43]. The DNA sequences of all plasmid inserts were verified by Sanger sequencing. Single-guided RNAs or shRNAs were packaged with psPAX2 (Addgene, 12260) and pMD2. G (Addgene, 12259) into HEK 293 T cells and were delivered to target cells by lentiviral transduction in the presence of 8 μg/ml polybrene. Cells were selected with puromycin for at least 3 weeks before experimental use.

For the luciferase reporter assay, 5×10^5 RAW 264.7 cells were transfected with 5 μg of Fcgr1-Luc or Fcgr4-Luc, 5–10 μg of expression vector, and 0.5 μg of pRL-TK Renilla luciferase control plasmid (Promega), followed by the indicated stimulations. Cells were lysed, and firefly luciferase activity was measured and normalized to *Renilla* luciferase activity following the manufacturer's instructions (Promega).

Expression and purification of recombinant proteins
Human importin α5 (aa 400–538) was cloned into the pGEX-4T1 GST fusion vector (Cytiva) and expressed by *Escherichia coli* BL21 (DE3) cells. GST-tagged proteins were purified with BeyoGold™ GST-tag Purification Resin (Beyotime) and eluted with 10 mM L-glutathione, followed by concentration with an Amicon Ultra15 filter (30-kD cutoff, Sigma). The synthesized ADAP NLS1 peptide (KEREKKREKEEKKRLELEKKEQKEKEKKEQEIKKK), ADAP NLS2 peptide (KAKTEEKDLKKLKKQEKEEKDFRKKFK), and STAT1 NLS peptide (HLQLKEQKNA) were purchased from Sangon.

Immunoblotting and Immunoprecipitation
Cells were lysed in lysis buffer (1% Triton X-100 (v/v) in 20 mM Tris-HCl (pH 8.3), 150 mM NaCl) supplemented with EDTA-free protease inhibitor cocktail (Roche). For immunoprecipitation experiments, cell lysates were precleared with protein G Sepharose beads (GE Healthcare) followed by incubation with antibodies at 4 °C overnight. Immunoprecipitates were resolved by SDS–PAGE, and immunoblotting was performed with the indicated primary antibodies. Immunoblots were developed with HRP- or IRDye-conjugated secondary antibodies and visualized by enhanced chemiluminescence or an Odyssey imaging system, respectively. For the GST pull-down assay, GST-importin α5 (aa 400–538) was incubated with cell lysates at 4 °C for 1 h, followed by coupling to GST-tagged purification resin overnight at 4 °C. Beads were then washed with lysis buffer and eluted in 1 × Laemmli sample buffer before being subjected to immunoblotting analysis.

Subcellular fractionation
Cytoplasmic and nuclear fractionation was performed using subcellular lysis buffer (250 mM sucrose, 20 mM HEPES (pH 7.4), 10 mM KCl, 150 mM MgCl₂, 1 mM EDTA, 1 mM EGTA) or nuclear lysis buffer (1% NP-40 (v/v) in 50 mM Tris-HCl (pH 8.3), 150 mM NaCl, 0.5% sodium deoxycholate, 0.1% SDS, 10% glycerol) supplemented with protease inhibitor cocktail as previously described [44]. Isolation of chromatin-bound proteins was performed using cytoskeletal buffer (10 mM PIPES-KOH (pH 6.8), 100 mM NaCl, 300 mM sucrose, 3 mM MgCl₂, 0.5 mM PMSF, 0.1 mM glycerolphosphate, 50 mM NaF, 1 mM Na₃VO₄, containing 0.1% Nonidet P-40 and protease inhibitor cocktail) as previously described [45].

Chromatin immunoprecipitation (ChIP) and biotin-labeled DNA pull-down assay
ChIP assays were performed as previously described [43]. DNA was purified from immunoprecipitates by STAT1 antibodies by phenol/chloroform extraction and used for PCR. The primers specific for the *Fcgr1* and *Fcgr4* promoters were: *Fcgr1*, sense 5′- CCGGAGTTAAGATCATCCTTGGCT-3′, antisense 5′- GGGCTGGGGACCAAGATTAGA-3′; *Fcgr4*, sense 5′- CTGATA-GACTCTCTGTGTGTCCCCG-3′, anti-sense 5′- CGGAACCCTTAAGGGCCCTAT-3′. Biotin-labeled DNA pull-down assays were performed as previously described with minor modifications [46]. Biotinylated *Fcgr4* promoter (−201 to −89) probes, putative STAT1-binding site-mutant probes, and

IL-2 promoter (−100 to −69) probes were synthesized by Sangon. The mutated probes for the putative STAT1-binding sites shown in the lower case were −191 TTTTCCTGGGG −181 to −191 ggggaagtttt −181 and −110 TTCTGGAAAA-101 to −110 ggagttcccc −101. Nuclear extracts were incubated with biotinylated promoter DNA at 4 °C overnight. The DNA-protein complexes were precipitated by streptavidin-conjugated agarose beads (Yeasen), washed with lysis buffer five times and boiled in 1 × Laemmli sample buffer before being subjected to immunoblotting analysis.

In situ Proximity Ligation Assay (PLA) and Immunofluorescence Microscopy
The interaction between ADAP and STAT1 was detected in formalin-fixed, paraffin-embedded (FFPE) spleen sections by PLA using a Duolink in situ detection kit (Sigma) according to the manufacturer's instructions. For immunofluorescence microscopy, FFPE tissue slides (5 μm) were deparaffinized and rehydrated with ethanol, followed by antigen retrieval in boiling citrate buffer (pH 6.0) for 20 min. After blocking in blocking solution for 30 min at 25 °C, the slides were incubated in primary antibodies overnight at 4 °C, followed by incubation in Alexa Fluor 647-conjugated anti-mouse IgG antibodies, Alexa Fluor 555-conjugated anti-rabbit IgG antibodies and Alexa Fluor 488-conjugated anti-CD68 for 1 h at 25 °C. Tissue autofluorescence was quenched by treatment with TrueBlack (Biotium) for 30 s. Nuclei were stained with DAPI solution. Imaging was performed at 40× or 60× magnification on a confocal microscope (Zeiss LSM 880) and analyzed with Zen software (Zeiss) and ImageJ.

Bioinformatics analysis
Gene expression datasets used to compare ADAP expression across peripheral blood T cells from ITP patients and healthy controls were previously published and are available from the National Center for Biotechnology Information Gene Expression Omnibus (GEO) database under accession numbers GSE46922 (new ITP $n = 7$; chronic ITP $n = 6$) [47], GSE574 (active ITP $n = 2$; control $n = 2$; remission $n = 2$) [14], GSE43177 (control $n = 10$, ITP $n = 9$) [48], and GSE56232 (new ITP $n = 6$; remission $n = 6$) [49]. The R package limma [50] (v3.42.2) was used to pool, remove batch effects and normalize data from the aforementioned datasets. Differential expression analyses were performed using the limma functions 'lmFit' and 'eBayes' and were defined based on a 1.5-fold change and adj. *P*-value < 0.05.

RNA-seq
Total RNA from splenic macrophages of WT and $Adap^{-/-}$ mice was extracted by TRIzol reagent (Ambion). RNA integrity and quantity were examined with an Agilent Bioanalyzer 2100 (Agilent). A sequencing library was prepared using the NEBNext Ultra RNA Library Prep Kit for Illumina. The mRNA was enriched using oligo (dT) magnetic beads, fragmented, and reversed-transcribed to cDNA using random hexamer primers and M-MuLV Reverse Transcriptase. Double strand cDNA was synthesized, adenine was added at the 3′ end, and the cDNA was ligated with sequencing adaptors. The fragments were purified with the AMPure XP system (Beckman Coulter), amplified by PCR and subjected to library quality control using the Agilent 2100 Bioanalyzer and ABI StepOnePlus Real-Time PCR System. Paired-end RNA sequencing was performed on an Illumina NovaSeq 6000 by Novogene, Tianjin. Sequenced reads (approximately 40 million clean reads per sample) were aligned to the mouse genome (mm10) using Hisat2 (v 2.0.5) and counted by featureCounts (v 1.5.0-p3). The differentially expressed genes between groups were quantified using DESeq2 (1.20.0). A 1.5-fold change and adjusted *P*-value < 0.05 were used for the identification of differentially expressed genes. The upregulated genes in $Adap^{-/-}$ macrophages were subjected to pathway enrichment analysis in KEGG, Reactome, DO, and DisGeNET pathways using the R package clusterProfiler (3.8.1), and pathways with a *P*-value < 0.05 were considered significantly enriched. Normalized read counts of all expressed genes were subjected to gene set enrichment analysis (GSEA) in GSEA software (Broad Institute & UC San Diego) using Molecular Signatures Database v.7.4 gene set collection. To determine the significance of gene set enrichment, a false discovery rate (FDR)-adjusted *P* value was calculated through 1000 permutations of random gene sets.

Quantitative RT–PCR
Total RNA was isolated from the cells using TRI reagent (Sigma). cDNA was prepared from RNA using RevertAid reverse transcriptase (Thermo Fisher) and oligo dT primers following the manufacturer's manual. Quantitative

PCR analysis and data collection were performed on a QuantStudio 5 Real-time PCR system (Thermo Fisher) using the primer pairs listed below. *Irf1*: forward, 5′-TAGGACGTGCTTTCACAGTCTAA-3′, reverse, 5′-GCATTCGAGTG ATTGGCATGG-3′; *Icam1*: forward, 5′-TCCGCTACCATCACCGTGTA-3′, reverse, 5′-TAGCCAGCACCGTGAATGTG-3′; *Cxcl9*: forward, 5′- GGAGTTCGAGGAACCC TAGTGA −3′, reverse, 5′- AGGCAGGTTTGATCTCCGTTC -3′; *Gapdh*: forward, 5′-GGGTCCCAGCTTAGGTTCATC-3′, reverse, 5′-ACTGTGCCGTTGAATTTGCC-3′. For the comparative analysis of gene expression levels, threshold cycle numbers of interest genes were normalized against the *Gapdh* gene and calculated with the ΔΔCt method.

Biacore analysis

The binding constants between purified proteins and peptides were measured by a single-cycle kinetics program on a Biacore T200 instrument (Cytiva) at 25 °C. The purified GST-importin α5 (aa 400–538) protein was immobilized on a Serie S CM5 sensor chip (Cytiva) to achieve approximately 5000 response units (RUs). Peptides were prepared in a series of twofold dilutions in HBS-EP + buffer (10 mM HEPES, 150 mM NaCl, 3 mM EDTA and 0.05% v/v Surfactant P20, Cytiva) from 206.89 nM to 12.93 nM. Peptides at increasing concentrations were injected sequentially at a flow rate of 30 μl/min for a contact phase of 180 s, followed by a dissociation phase of 900 s without regeneration. All data were analyzed using Biacore T200 evaluation software.

Statistical analysis

All data were analyzed with GraphPad Prism 7 or the indicated packages with R. Data are presented as the mean ± SEM. For the comparison between two group means, a two-tailed unpaired Student's t-test or Mann–Whitney U test for nonparametric data was used. For the comparison of more than two groups, a one-way or two-way ANOVA followed by Tukey's, or Sidak's multiple comparison test was used as indicated specifically. P values are as follows: *$P < 0.05$; **$P < 0.01$; ***$P < 0.001$; ****$P < 0.0001$; ns, nonsignificant.

RESULTS

ADAP underexpression in splenic tissue is associated with thrombocytopenia, which is reversed by macrophage depletion

To demonstrate a direct association of ADAP with ITP in human patients, the expression of ADAP was first analyzed in splenic tissue sections from ITP patients who underwent splenectomy. Splenic tissues from non-ITP patients with splenic trauma were used as controls. Immunofluorescence imaging showed that the overall expression of ADAP and that of ADAP within splenic macrophages (CD68^{+}) was greatly reduced in ITP spleens compared to trauma controls (Fig. 1A). We further analyzed the ADAP transcript levels from different clinical subgroups of ITP patients using publicly available mRNA microarray datasets and found that ADAP expression was significantly lower in peripheral blood T cells in patients with new and chronic ITP, whereas in patients in remission, the level of ADAP was comparable to that in the controls (Fig. 1B). Thus, ITP patients had significantly reduced expression levels of ADAP. Moreover, we compared the circulating platelet and reticulated platelet counts among wild-type (WT), *Adap*^{−/−} and *Skap1*^{−/−} mice. Src family-associated phosphoprotein 1 (SKAP1) is a bona fide ADAP interacting partner. While SKAP1 deficiency does not lead to loss of ADAP, loss of ADAP causes SKAP1 deficiency in both cells and gene-KO mice [30, 51]. Platelet counts in *Adap*^{−/−} mice were significantly reduced as compared to WT controls, while those in *Skap*^{−/−} mice was comparable to that in WT mice (Fig. 1C), suggesting that the deficiency of ADAP but not SKAP1 contributes to thrombocytopenia. Although the absolute number of reticulated platelets was lower in *Adap*^{−/−} mice than in WT mice ($22 \pm 2 \times 10^9$/l vs. $40 \pm 3 \times 10^9$/l), the percentage of reticulated platelets was similar between these mice (Fig. 1C). These data suggest that underexpression of ADAP is associated with thrombocytopenia.

Anti-platelet antibody-mediated platelet phagocytosis plays a key role in the immune pathophysiology of ITP [8]. To investigate whether antibody-dependent platelet clearance was affected in *Adap*^{−/−} mice, we compared the thrombocytopenia between WT and *Adap*^{−/−} mice in a mouse ITP model induced by subcutaneous administration of anti-platelet antibody R300 (anti-CD42b/GPIbα), wherein platelets are cleared mainly in the spleen [52]. As shown in Fig. 1D, while subcutaneous injection of R300 at 0.16 mg/kg rapidly reduced the platelet counts in both WT and *Adap*^{−/−} mice to a similar extent, a reduced dose as low as 0.08 mg/kg triggered a more rapid reduction in platelet counts in *Adap*^{−/−} mice than in WT mice. Further, similar results were obtained with the transfusion of R300-opsonized and cell tracker dye DiI-labelled platelets into either WT or *Adap*^{−/−} mice via the tail vein. The percentages of remaining R300-opsonized platelets in the peripheral blood were significantly lower in *Adap*^{−/−} mice than in WT mice at 5 min post-injection (Fig. 1E). Interestingly, when an anti-platelet antibody of IgG1 subtype MWReg30 (anti-GPIIb) was used to trigger passive ITP, platelet counts in both WT and *Adap*^{−/−} mice dropped to the same extent (Supplementary Fig. 1B). Unexpectedly, the levels of platelet-associated antibodies were comparable between WT and *Adap*^{−/−} mice (Supplementary Fig. 1C), suggesting ADAP deficiency may sensitize the macrophage to antibody-opsonized platelets for phagocytosis rather than increase the level of autoantibody against platelets.

Next, to identify the cells most responsible for the enhanced platelets destruction upon ADAP deficiency, we examined the effects of systemic depletion of various immune cells on platelet counts in *Adap*^{−/−} mice. Compared to the PBS control, a single dose of clodronate liposomes that depleted macrophages significantly (Supplementary Fig. 1D) restored the platelet counts in *Adap*^{−/−} mice to a level comparable to that in WT mice within 1 day following injection and was sustained over a time course of 4 days (Fig. 1F). In contrast, in vivo depletion of B cells and CD4^{+} T cells by anti-CD20 and anti-CD4 antibodies, respectively, had little effect on the platelet counts in *Adap*^{−/−} mice (Fig. 1G). Depletion of CD8^{+} T cells by anti-CD8a also gradually increased the platelet numbers on day 3 after the initial dose, albeit to a lower level than macrophage depletion. Thus, these results suggest that macrophages but not CD4^{+} T cells or B cells play a key role in heightened platelet clearance accounting for the mild thrombocytopenia in *Adap*^{−/−} mice.
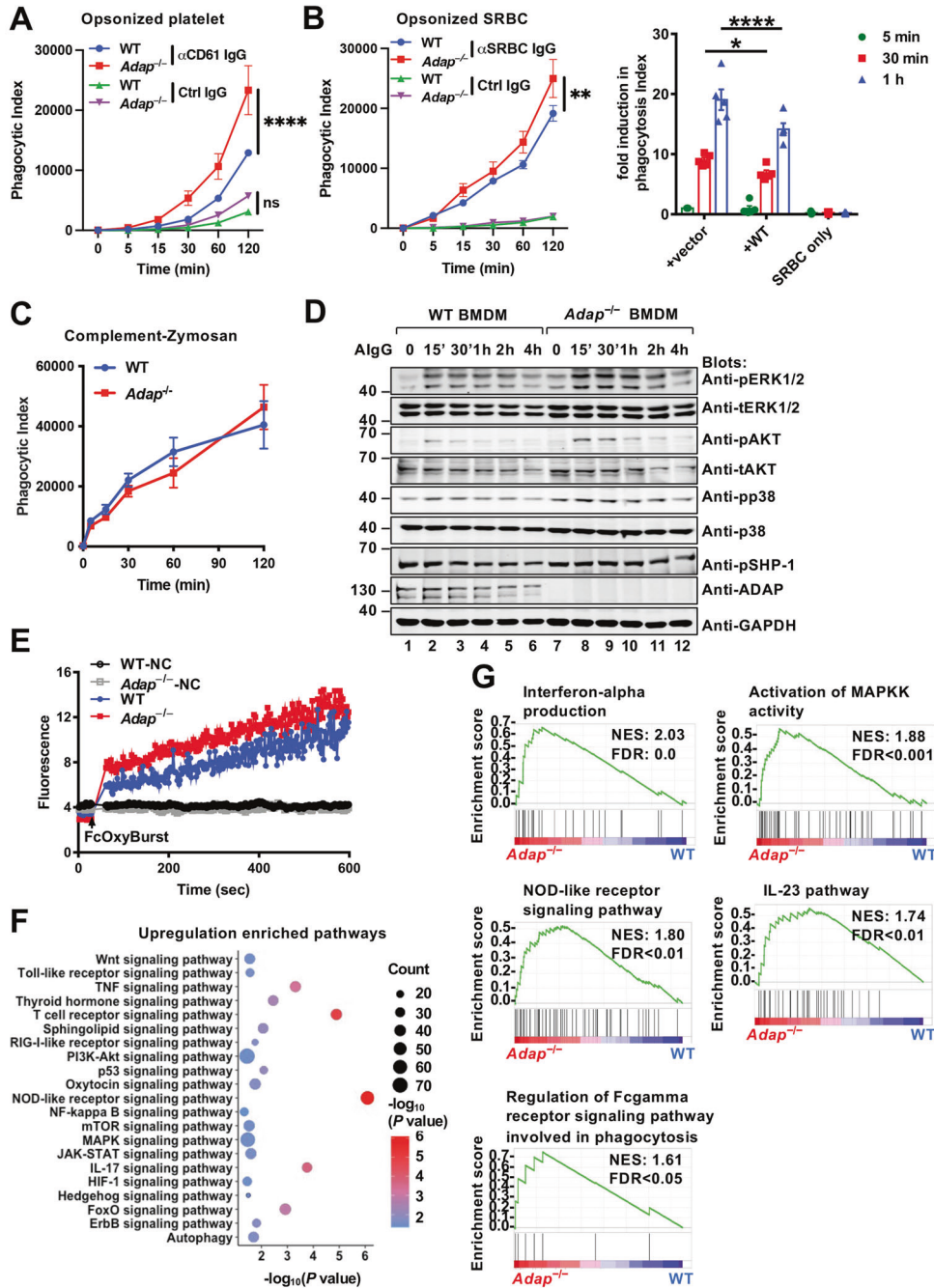
Adap^{−/−} macrophages exhibit enhanced FcγR-dependent phagocytic ability and upregulated proinflammatory signaling

FcγRs and complement receptors (CRs) are the two best described opsonic receptors for macrophage phagocytosis [53]. We thus assessed the effect of ADAP deficiency on FcγR- or CR-mediated macrophage phagocytosis. Macrophages prepared from WT and *Adap*^{−/−} mice were subjected to phagocytosis assays with IgG-opsonized platelet and sheep red blood cells (SRBCs) or complement-opsonized Alexa Fluor 488-conjugated zymosan A particles. As expected, the accelerated platelet clearance in *Adap*^{−/−} mice was accompanied by an enhanced phagocytic capacity of macrophages, as shown by the phagocytosis of anti-platelet IgG-opsonized platelets by *Adap*^{−/−} peritoneal macrophages being significantly higher than that by WT (Fig. 2A and Supplementary Fig. 2A, B). Similar results were observed in the phagocytosis of anti-SRBC IgG-opsonized SRBCs by *Adap*^{−/−} bone marrow-derived macrophages (BMDMs) (Fig. 2B). Furthermore, reconstitution of stable ADAP knockout macrophages with WT ADAP significantly blunted the uptake of IgG-opsonized SRBC after 30 min to 1 h of incubation (Fig. 2B, right panel). In contrast, the uptake of complement-opsonized Alexa Fluor 488-conjugated zymosan A particles by WT and *Adap*^{−/−} BMDMs was comparable (Fig. 2C). This indicates that the increased platelet destruction by *Adap*^{−/−} macrophages occurs through FcγR- but not CR-mediated macrophage phagocytosis.

Next, we asked whether the enhanced FcγR-mediated phagocytosis in *Adap*^{−/−} macrophages is accompanied by a change in signaling downstream of FcγRs. Stimulation of FcγRs by
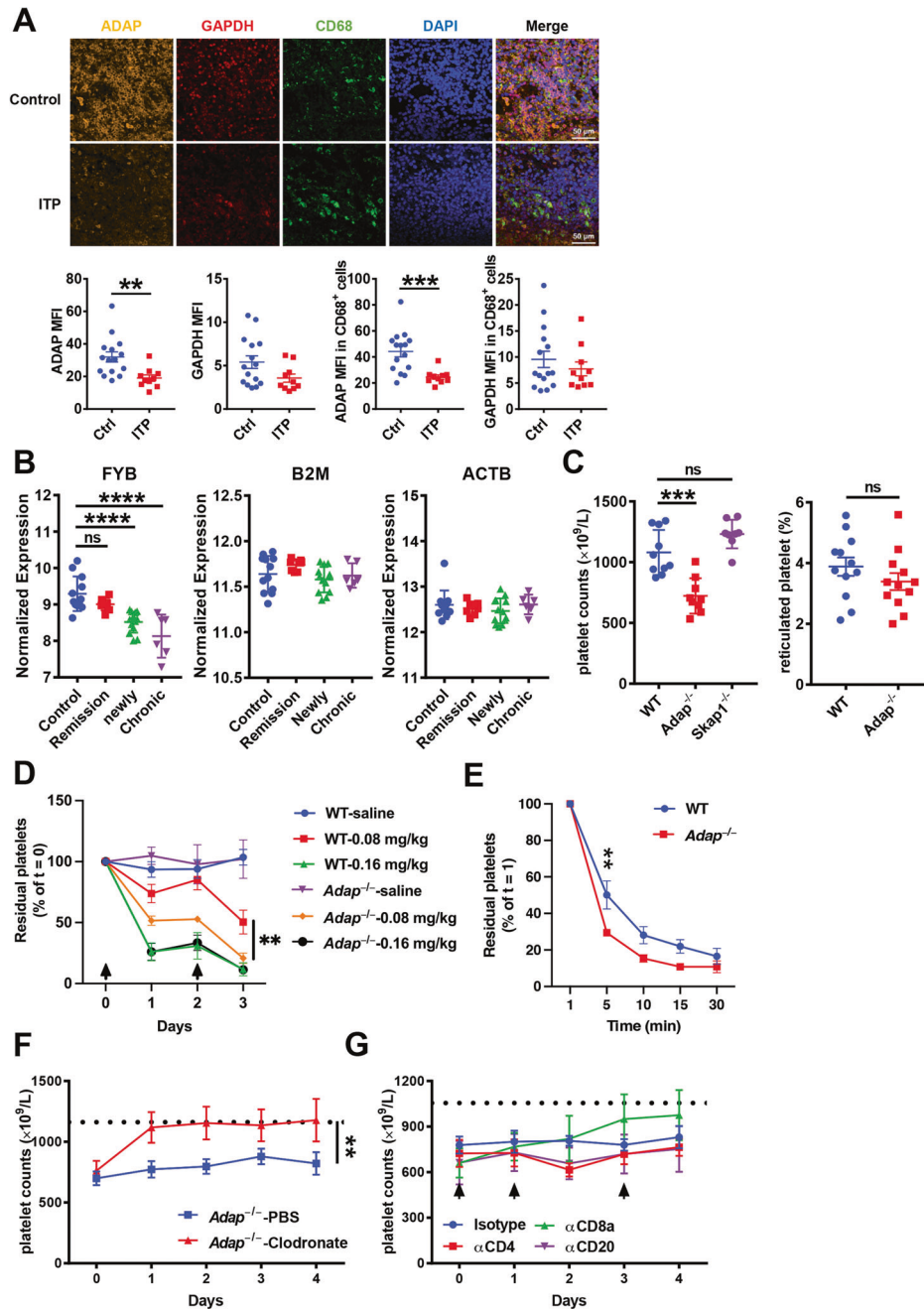
Fig. 1 ADAP underexpression in splenic tissue is associated with thrombocytopenia, which is reversed by macrophage depletion. **A** Representative images of splenic tissue samples from ITP patients ($n = 10$) or trauma controls ($n = 15$) stained with antibodies against ADAP, GAPDH and CD68. Scale bars, 50 μm. The mean fluorescence intensity (MFI) of each sample (over 15 images in each sample, Mann–Whitney U test and unpaired t test) was plotted. **B** ADAP mRNA expression in healthy controls ($n = 12$), ITP patients in remission ($n = 8$), patients with new ITP ($n = 13$), and chronic ITP ($n = 6$). Publicly available mRNA microarray datasets on peripheral T-cells under accession number GSE46922, GSE574, GSE43177, and GSE56232 were obtained from GEO and pooled. Statistics analysis used the limma package and linear fit and eBayes statistics in R. **C** Circulating platelet counts and reticulated platelet percentages in WT mice ($n = 10$), $Adap^{-/-}$ mice ($n = 9$), and $Skap1^{-/-}$ mice ($n = 8$, one-way ANOVA, Tukey's multiple comparison). **D** WT and $Adap^{-/-}$ mice were treated with saline, or anti-mouse GPIbα antibody R300 (anti-CD42b, IgG mixture) at the indicated doses via s.c. on days 0 and 2 ($n = 4$ mice in each group, two-way ANOVA, Tukey's multiple comparison). Platelet counts were enumerated over a time course of 3 days and presented as percentages of those prior to antibody injection on Day 0. **E** In vivo platelet clearance in WT and $Adap^{-/-}$ mice transfused with DiI-labeled R300-opsonized platelet ($n = 5$ each, two-way ANOVA, Sidak's multiple comparison). The percentages of DiI-labeled R300-opsonized platelets in total platelets were determined at 1, 5, 10, 15, and 30 min post-transfusion and presented as the percentages of those at 1 min. **F** Platelet counts in clodronate-liposome- or PBS-liposome-treated $Adap^{-/-}$ mice (clodronate-liposome, $n = 8$; PBS-liposome, $n = 7$, paired t-test) over a time course of 4 days after treatment. The horizontal dashed line represents the baseline platelet count of WT mice examined in parallel ($n = 4$). **G** Platelet counts in $Adap^{-/-}$ mice treated with isotype, anti-CD4, anti-CD8a, or anti-CD20 antibodies ($n = 4$ mice each) over a time course of 4 days. Arrowheads indicate the injections given on days 0, 1, and 3. The horizontal dashed line represents the baseline platelet count of WT mice examined in parallel ($n = 4$). **$P < 0.01$; ***$P < 0.001$; ****$P < 0.0001$; ns, nonsignificant

Fig. 2 $Adap^{-/-}$ macrophages exhibit enhanced FcγR-dependent phagocytic ability and upregulated proinflammatory signaling. **A** Phagocytosis of DiI-labeled anti-CD61 IgG- or isotype control IgG-opsonized platelets by peritoneal macrophages prepared from WT mice and $Adap^{-/-}$ mice ($n = 6$ for anti-CD61 IgG, $n = 4$ for IgG ctrl, two-way ANOVA, Tukey's multiple comparison). The phagocytic index was calculated as the mean fluorescence intensity multiplied by the frequency of DiI-positive cells. **B** Phagocytosis of PKH26-labeled anti-SRBC IgG- or isotype control IgG-opsonized SRBCs by macrophages. Left panel, BMDMs prepared from WT mice and $Adap^{-/-}$ mice ($n = 8$ for anti-SRBC IgG, $n = 4$ for IgG ctrl, two-way ANOVA, Tukey's multiple comparison) were subjected to phagocytosis assay as assessed by flow cytometry and presented as phagocytic index. Right panel, ADAP KO RAW 264.7 cells stably reconstituted with either empty vector or ADAP WT construct ($n = 5$ each, two-way ANOVA, Tukey's multiple comparison) were subjected to phagocytosis assay with PKH26-labeled IgG-opsonized SRBC, and fold induction in phagocytic index was calculated by dividing the value of each group by those of empty vector-transfected cells at 5 min. **C** Phagocytosis of complement-opsonized Alexa Fluor 488-conjugated zymosan A particles by WT and $Adap^{-/-}$ ($n = 6$ mice each) BMDMs. **D** Immunoblot analysis of ERK1/2, AKT, p38 and SHP-1 phosphorylation in WT and $Adap^{-/-}$ BMDMs stimulated for the indicated time points with aggregated IgG (AIgG). **E** BMDMs from WT and $Adap^{-/-}$ mice ($n = 11$ mice each) were either left unstimulated (WT-NC and $Adap^{-/-}$-NC) or stimulated with FcOxyBurst reagent, and the development of green fluorescence was monitored by flow cytometry over a 10 min period. Each dot represents the mean value from three independent experiments. **F** Significantly enriched signaling pathways from the upregulated genes in $Adap^{-/-}$ macrophages relative to WT macrophages. The dot size indicates the number of genes enriched in each pathway, while the dot color indicates the statistical significance of the enrichment. **G** GSEA of the indicated datasets in $Adap^{-/-}$ macrophages relative to WT macrophages. Normalized enrichment score (NES) and the FDR q-value of each enrichment are shown. *$P < 0.05$; **$P < 0.01$; ****$P < 0.0001$; ns, nonsignificant

aggregated IgG (AIgG) induced higher levels of ERK1/2, AKT, and p38 phosphorylation in $Adap^{-/-}$ BMDMs than in WT BMDMs, without affecting the phosphorylation of SHP-1 phosphatase (Fig. 2D). Moreover, following FcγR engagement with the H_2DCF-labeled BSA immune complex, $Adap^{-/-}$ BMDMs displayed a more robust oxidative burst than WT BMDMs (Fig. 2E). RNA-Seq analysis of splenic macrophages from WT mice and $Adap^{-/-}$ mice revealed that multiple proinflammatory signaling pathways were enriched among the upregulated genes in $Adap^{-/-}$ splenic macrophages relative to WT macrophages (Fig. 2F). In addition, the significant enrichment of NOD-like receptor (NLR) signaling and the IL17/23 signaling pathway in $Adap^{-/-}$ macrophages were further confirmed by GSEA using all genes expressed instead of differentially expressed genes for calculation (Fig. 2G). These data suggested that ADAP deficiency induces a high FcγR-dependent phagocytic ability of macrophages with a proinflammatory phenotype.

ADAP deficiency selectively promotes the transcription and expression of STAT1-targeted genes *Fcgr1* and *Fcgr4*

Four types of FcγRs, FcγRI, FcγRIIB, FcγRIII, and FcγRIV, are expressed on monocytes and macrophages in mice [12]. We examined the impact of ADAP deficiency on the expression levels of each type of FcγR on macrophages. Splenic macrophages isolated from WT or $Adap^{-/-}$ mice were either left untreated or stimulated with IFN-γ, followed by flow cytometric analysis of FcγR expression. As shown in Fig. 3A, while there was no statistically significant difference in the expression of FcγRIII and the inhibitory FcγRIIB between WT and $Adap^{-/-}$ splenic macrophages regardless of IFN-γ stimulation, the expression of FcγRI and FcγRIV was significantly higher in $Adap^{-/-}$ splenic macrophages than in WT splenic macrophages in response to IFN-γ stimulation. Furthermore, knockdown of ADAP with shRNAs (shADAP) significantly increased *Fcgr1* promoter-driven luciferase activity in RAW 264.7 cells in response to IFN-γ stimulation, which was blunted by mutations of the two classical STAT1 binding-γ-activated sequence (GAS) elements on the *Fcgr1* promoter (from −189 to +1) [39] (Fig. 3B).

It is not known whether STAT1 can bind to the *Fcgr4* promoter and regulate transcription of the *Fcgr4* gene. Two putative STAT1-binding sites, −191 TTTTCCTGGGG −181 and −110 TTCTGGAAAA-101, were found in the promoter of the *Fcgr4* gene by the GPMiner [54] program. Knockdown of ADAP with shADAP markedly increased the transcription of the *Fcgr4* promoter compared to the shEGFP controls, which was largely abolished upon mutations of these two STAT1-binding sites in the promoter (Fig. 3C). Furthermore, a DNA pull-down assay showed that pY701-STAT1 could bind to WT biotinylated *Fcgr4* promoter probes but not probes with mutations at putative STAT1-binding sites. In comparison, the amount of DNA-pY701-STAT1 complexes was significantly higher in ADAP KO RAW 264.7 cells than in control cells (Fig. 3D). Sequential chromatin immunoprecipitation (ChIP)-PCR analysis also confirmed the IFN-γ-induced binding of STAT1 to the *Fcgr1* and *Fcgr4* promoters in vivo, wherein the amount of *Fcgr1* or *Fcgr4* promoter DNA pulled down by the anti-STAT1 antibody was significantly higher in ADAP KO RAW 264.7 cells than in controls following IFN-γ stimulation (Fig. 3E). These data indicate that ADAP deficiency selectively elevates the STAT1-dependent transcription and expression of FcγRI and FcγRIV.

### ADAP interacts with STAT1 and modulates STAT1 nuclear translocation

An increase in IFN-γ is one of the major characteristics of some ITPs [16, 17]. The biological activity of IFN-γ is mediated by the transcription factor STAT1, indicating that STAT1 could act as one of the crucial effectors in ADAP deficiency-driven ITP. We next examined a potential physical interaction between ADAP and STAT1. While the overall STAT1 expression levels in splenic macrophages were comparable between ITP and trauma controls (Fig. 4B),

proximity ligation assays using anti-ADAP and anti-STAT1 antibodies showed that ADAP interacted with STAT1 in human splenic tissues (Fig. 4A). In addition, the interaction between endogenous ADAP and STAT1 was examined in RAW264.7 cells, where IFN-γ stimulation increased the amount of pY701-STAT1 coprecipitated by anti-ADAP, which peaked at 15 min and declined thereafter (Fig. 4C). In line with this observation, ectopically expressed ADAP also bound to STAT1 in HEK 293 T cells, where ADAP is not constitutively present. The binding sites were mapped to a region spanning residues 231 to 340 on the N-terminus of ADAP (Fig. 4D) and the coiled-coil domain (CCD) of STAT1 (Fig. 4E).

We next assessed whether ADAP is required for IFN-γ-mediated STAT1 activation hallmarked by the induction of STAT1 phosphorylation at the Y701 and S727 sites. Western blot analysis showed that the level of IFN-γ-induced STAT1 phosphorylation at both the Y701 and S727 sites was comparable between control and stable ADAP KO RAW 264.7 cells (Fig. 4F). Further, as shown in Fig. 4G, H, loss of ADAP increased the levels of pY701-STAT1 and total STAT1 in the nuclear fraction as well as in the chromatin-bound fraction following IFN-γ stimulation. Conversely, overexpression of ADAP reduced the amount of chromatin-bound pY701-STAT1 (Supplementary Fig. 3A). In line with these observations, in response to IFN-γ, the mRNA expression levels of STAT1-targeting genes, including *Irf1*, *Icam1* and *Cxcl9*, were further increased in $Adap^{-/-}$ BMDMs compared to WT controls (Fig. 4I). Thus, while having no effect on STAT1 tyrosine phosphorylation, ADAP deficiency facilitates the nuclear translocation of STAT1, which consequently leads to an enhancement of transcription of its targeted genes in macrophages.

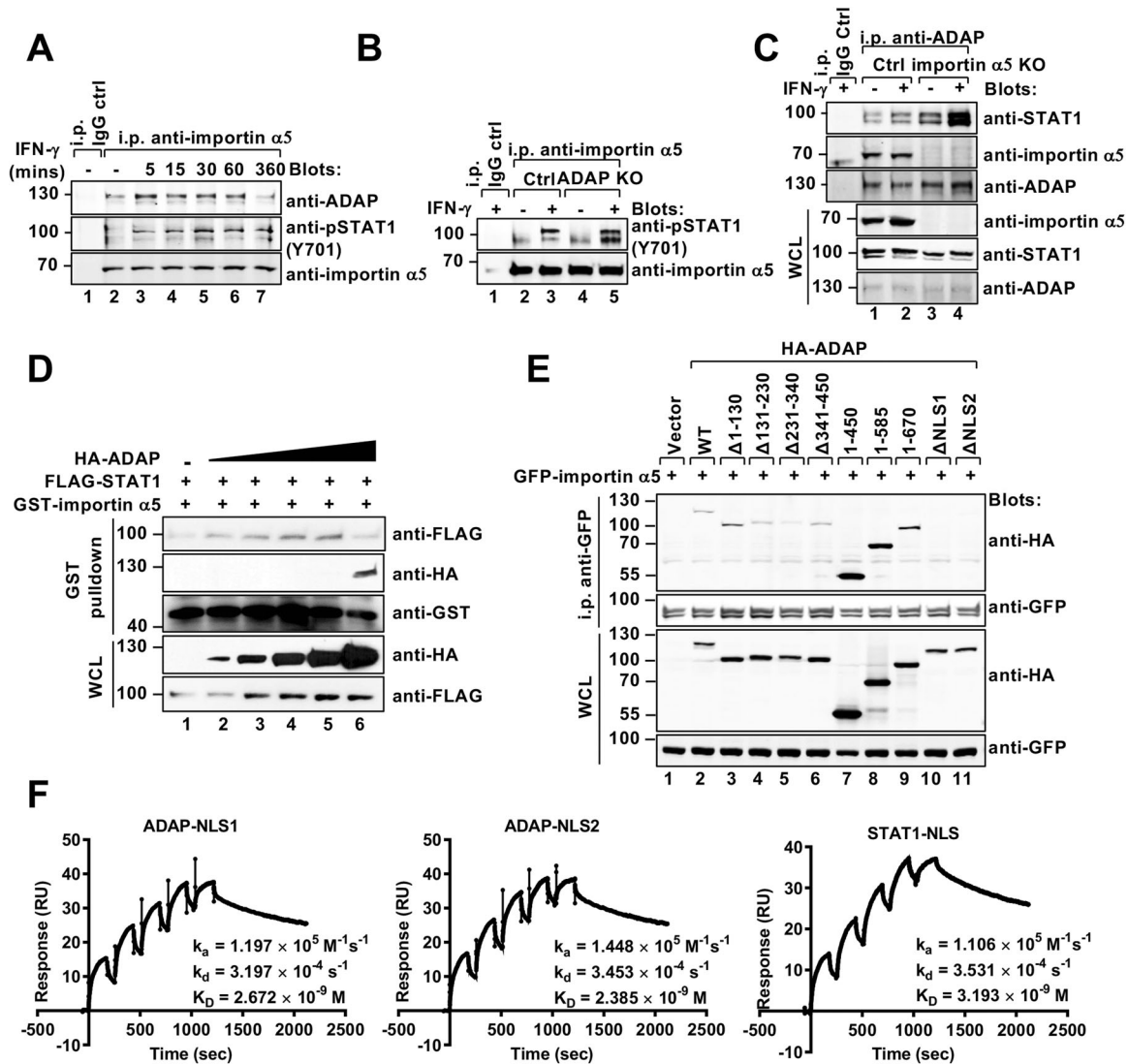### ADAP competes with STAT1 for importin α5 binding

Nuclear transport of pY-STAT1 following IFN stimulation hinges on a subset of the karyopherin alpha family, among which importin α5 (also known as KPNA1) binds to pY-STAT1 via a noncanonical nuclear localization sequence (NLS) in the DNA binding domain of STAT1 [20, 21]. Interestingly, ADAP also consists of two putative NLSs, which span residues 469–505 and residues 674–700 and resemble the bipartite nuclear localization motifs KR/RR-X$_{11–12}$-KK/RK found in nuclear proteins [55–57]. Coimmunoprecipitation assays showed that both pY-STAT1 and ADAP were readily detected in the immunoprecipitates by anti-importin α5, and IFN-γ stimulation increased their binding at an early time point of 5 min (Fig. 5A), suggesting that there exists a triple complex of ADAP-importin α5-STAT1. Interestingly, in ADAP KO Raw 264.7 cells, the amount of pY-STAT1-importin α5 complex was significantly higher than in the controls (Fig. 5B). On the contrary, overexpression of ADAP decreased the amount of pY-STAT1-importin α5 complex (Supplementary Fig. 3B). Further, depletion of importin α5 using CRISPR–Cas9 in Raw 264.7 cells markedly increased the binding between ADAP and STAT1 (Fig. 5C). Furthermore, in vitro binding competition experiments were performed by mixing purified GST-importin α5 (aa 400–538) protein, which is known for STAT1 binding [58], with cell lysates from HEK 293 T cells transfected with FLAG-STAT1 and increasing amounts of HA-ADAP. Substantial amounts of FLAG-STAT1 but not HA-ADAP were pulled down by GST-importin α5 in the presence of HA-ADAP at low concentrations. The addition of HA-ADAP at a high concentration greatly reduced the level of FLAG-STAT1 pulled down by GST-importin α5 (Fig. 5D). These data suggest that ADAP and STAT1 bind mutually and competitively to importin α5. Our previous study showed ADAP interacts with another STAT family member STAT3 in response to TLR activation. However, in contrast to importin α5-STAT1, the complex formation of importin α5-STAT3 was fewer in ADAP KO than in WT Raw 264.7 cells in response to IL-6 stimulation (Supplementary Fig. 3C), suggesting ADAP may specifically compete with STAT1 for importin α5 binding. Moreover, truncation mutants of ADAP lacking STAT1-binding sites (residues 231–340) and NLS1/NLS2 motifs showed reduced binding with importin α5, suggesting that NLS1 and NLS2 motifs in ADAP are responsible for
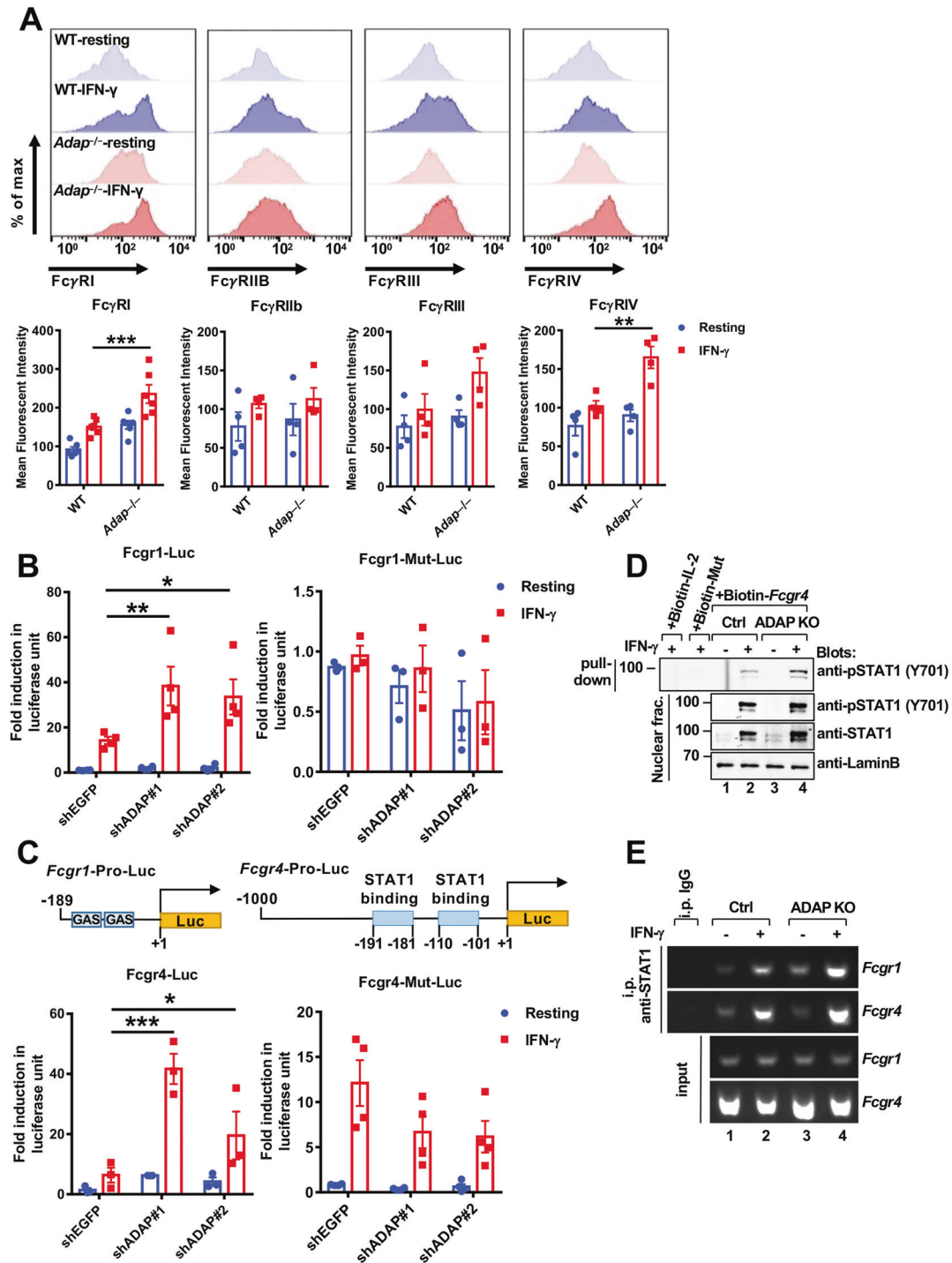
Fig. 3 ADAP deficiency selectively promotes the transcription and expression of STAT1-targeted genes *Fcgr1* and *Fcgr4*. **A** FcγR expression on resting and IFN-γ-treated splenic macrophages. Representative histogram by FACS analysis of FcγRI, FcγRIIB, FcγRIII, and FcγRIV on splenic macrophages from WT and *Adap*⁻/⁻ mice (*n* = 4 mice each). Splenocytes were either left unstimulated or stimulated with 10 ng/ml IFN-γ for 18 h. F4/80-positive macrophages were gated out and assessed for FcγR expression. Mean fluorescence intensity was plotted (two-way ANOVA, Sidak's multiple comparison). **B, C** Luciferase activity of RAW 264.7 cells transfected with shADAP or shEGFP, together with Fcgr1-Luc or STAT1-binding site mutant-containing Fcgr1-Mut-Luc (**B**, *n* ≥ 3, two-way ANOVA, Tukey's multiple comparison), or Fcgr4-Luc or STAT1-binding site mutant-containing Fcgr4-Mut-Luc reporters (**C**, *n* ≥ 3, two-way ANOVA, Tukey's multiple comparison), followed by stimulation with IFN-γ for 6 h. Schematic diagrams of the reporter constructs are shown in the intermediate panels. **D** Immunoblot analysis of the biotinylated *Fcgr4* promoter probe pull-down precipitates from WT and *Adap*⁻/⁻ iBMM cells. Cells were either left unstimulated or stimulated with IFN-γ for 1 h. Nuclear fractions were extracted and incubated with either biotinylated IL-2 promoter as a control, STAT1-binding site mutant-containing *Fcgr4* promoter probes (Biotin-Mut) or WT *Fcgr4* promoter probes. The biotinylated DNA-protein complexes were pulled down using streptavidin-conjugated agarose beads and subjected to immunoblotting analysis. **E** ChIP-PCR analysis of the interactions between STAT1 and the *Fcgr1* and *Fcgr4* promoters in WT and *Adap*⁻/⁻ iBMM cells. The *Fcgr1* and *Fcgr4* promoters were amplified with PCR from the precipitated DNA by anti-STAT1 antibodies. *P < 0.05; **P < 0.01; ***P < 0.001
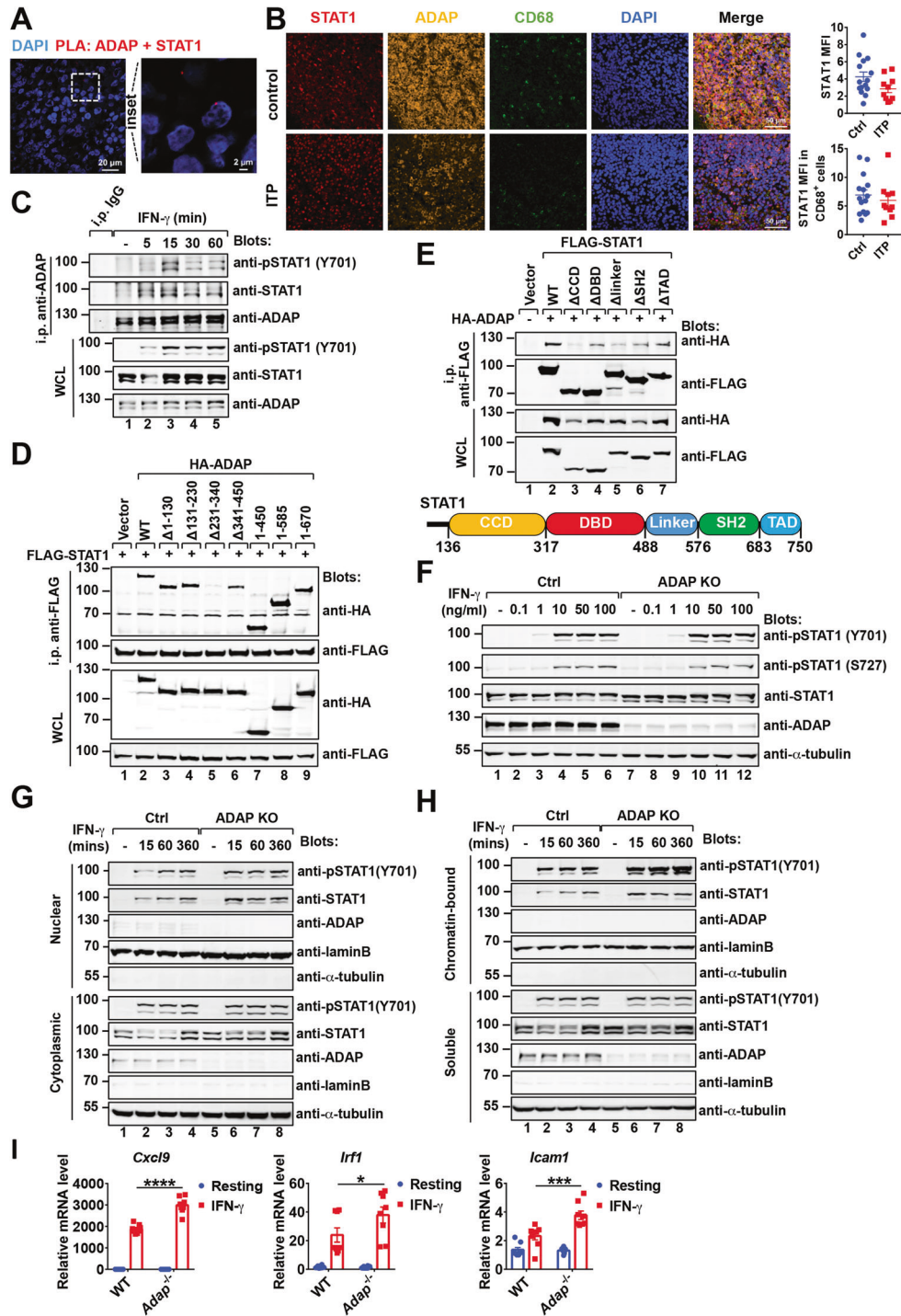
Fig. 4 ADAP interacts with STAT1 and modulates STAT1 nuclear translocation. **A** Proximity ligation assay of ADAP and STAT1 in splenic tissue samples from trauma controls. Representative images are shown at 60 × (left) and higher (right inset) magnification. **B** Immunofluorescence of STAT1 and ADAP in spleen tissue samples from ITP patients ($n = 10$) or trauma controls ($n = 15$). Macrophages were stained with Alexa Fluor 488-conjugated anti-CD68. Scale bars, 50 μm. The mean fluorescence intensity (MFI) of each sample (over 15 images in each sample) was plotted. **C** ADAP binds to STAT1 in macrophages. RAW 264.7 cells were stimulated with 10 ng/ml IFN-γ for the indicated time and subjected to immunoprecipitation with anti-ADAP antibodies followed by immunoblotting with the indicated antibodies. **D** FLAG-STAT1 was coexpressed with empty vector, HA-ADAP WT, or HA-ADAP truncation mutants in HEK 293 T cells. Cell lysates were subjected to immunoprecipitation using an anti-FLAG antibody, followed by blotting with anti-HA and anti-FLAG antibodies. **E** HEK 293 T cells were transfected with HA-ADAP together with either empty vector, FLAG-STAT1 WT, or FLAG-STAT1 truncation mutants as indicated. Immunoprecipitation was performed using an anti-FLAG antibody, followed by blotting with anti-HA and anti-FLAG antibodies. A schematic diagram of STAT1 protein domains is shown in the lower panel. **F** Immunoblot analysis of STAT1 phosphorylation in control or ADAP KO RAW264.7 cells that were stimulated with IFN-γ at the indicated dose for 30 min. **G, H** Immunoblot analysis of pY701-STAT1, STAT1 and ADAP in cytoplasmic and nuclear fractions (**G**) or soluble and chromatin-bound fractions (**H**) in control or ADAP KO RAW264.7 cells. Cells were stimulated with IFN-γ at the indicated time points and subjected to cellular fractionation. **I** Relative mRNA levels of STAT1 regulatory genes in BMDMs from WT and *Adap*⁻/⁻ mice ($n = 8$ mice each, two-way ANOVA, Sidak's multiple comparison). Relative mRNA levels were normalized to *Gapdh*. *$P < 0.05$; ***$P < 0.001$; ****$P < 0.0001$

Fig. 5 ADAP competes with STAT1 for importin α5 binding. **A** Importin α5 interacts with both ADAP and STAT1 in response to IFN-γ in RAW264.7 cells. RAW264.7 cells were stimulated with IFN-γ for the indicated time points, and the interaction between importin α5 and ADAP or phosphor-STAT1 was determined by immunoprecipitation with anti-importin α5, followed by immunoblotting with antibodies against ADAP and pY701-STAT. **B** The effects of ADAP deficiency on the interaction between STAT1 and importin α5. WT or ADAP-KO RAW264.7 cells were treated with or without IFN-γ as indicated. The interaction between STAT1 and importin α5 was determined by immunoprecipitation with anti-importin α5, followed by immunoblotting with pY701-STAT1 antibody. **C** Immunoprecipitation and immunoblot analysis of the ADAP/STAT1 interaction in control or importin α5 KO RAW264.7 cells with or without IFN-γ stimulation. **D** Competitive in vitro binding of ADAP and STAT1 to importin α5 by GST pulldown assay. HEK 293 T cells were transfected with equal amounts of FLAG-STAT1 constructs and increased amounts of HA-ADAP constructs. Cell lysates were incubated with equal amounts of purified GST-importin α5 (aa 400–538) protein, followed by pull-down with GST-tag purification resin. The precipitates were subjected to immunoblot analysis with anti-HA and anti-FLAG antibodies. **E** GFP-importin α5 was coexpressed with empty vector, HA-ADAP WT, or HA-ADAP truncation mutants in HEK 293 T cells. Cell lysates were subjected to immunoprecipitation using anti-GFP antibody, followed by blotting with anti-HA and anti-FLAG antibodies. **F** Surface plasmon resonance analysis of the purified importin α5 (aa 400–538) interactions with ADAP NLS1, NLS2 or STAT1 NLS peptide

importin α5 binding and that the interaction between ADAP and STAT1 is also required for ADAP binding to importin α5 (Fig. 5E). Surface plasmon resonance analysis (BIAcore) showed that comparable with the NLS of STAT1 [59, 60], the NLS1 and NLS2 of ADAP bound to GST-importin α5 (aa 400–538) with similar high affinities, showing equilibrium dissociation constant (K_D) of 2.672 nM and 2.385 nM, respectively (Fig. 5F).

Targeting the STAT1-importin α5 interaction or STAT1 activity mitigates thrombocytopenia in _Adap_^−/− mice
Given that ADAP deficiency led to heightened macrophage phagocytosis by promoting STAT1 nuclear translocation, we reasoned that pharmacologically inhibiting STAT1 activity may

mitigate thrombocytopenia in ADAP-deficient mice. Fludarabine as a nucleoside analog has been widely used as STAT1-inhibitor, where it causes a sustained loss of STAT1 protein and mRNA but not of other STATs [61]. As shown in Fig. 6A, a daily dose of fludarabine treatment significantly elevated the peripheral platelet counts in _Adap_^−/− mice to a level comparable to that in WT mice after 6 days. This result confirms that the decreased platelet counts caused by ADAP deficiency can be mitigated by inhibiting STAT1.

Furthermore, we tested whether targeting the STAT1-importin α5 interaction could also ameliorate mild thrombocytopenia in _Adap_^−/− mice. Ivermectin is a multitargeted drug with anti-parasitic and anti-viral activities [62]. Specifically, Ivermectin
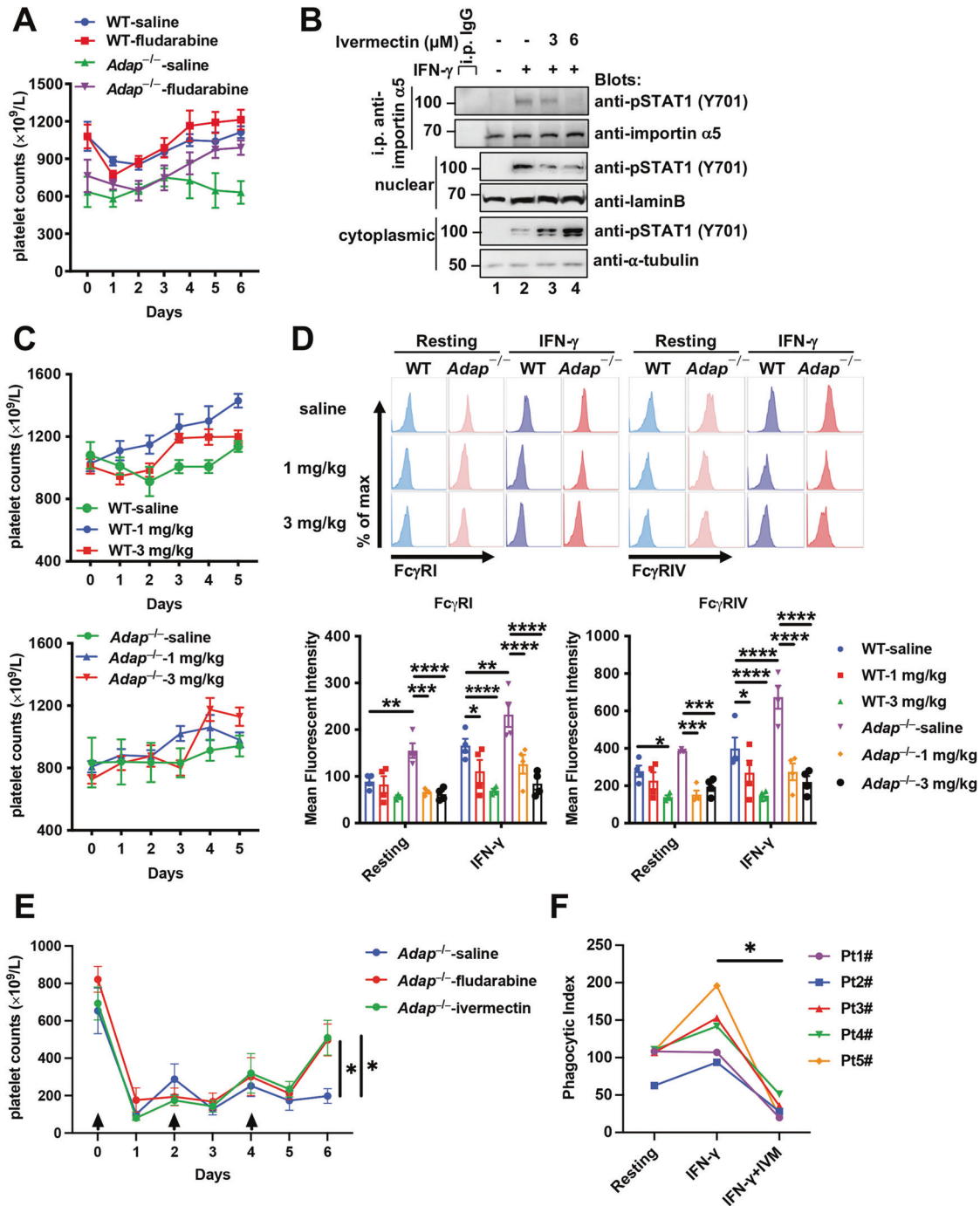
Fig. 6 Targeting the STAT1-importin α5 interaction or STAT1 activity mitigates thrombocytopenia in $Adap^{-/-}$ mice. **A** Platelet counts in WT and $Adap^{-/-}$ mice ($n = 4$ mice each) treated with fludarabine (50 mg/kg) or saline over a time course of 6 days. **B** Ivermectin disrupts the STAT1-importin α5 interaction and impairs STAT1 nuclear localization. RAW264.7 cells were primed with the indicated doses of ivermectin before stimulation with IFN-γ for 30 min and subjected to immunoprecipitation analysis with anti-importin α5 and immunoblot analysis of pY701-STAT1 in cytoplasmic and nuclear fractions. **C** Platelet counts in WT (upper panel) and $Adap^{-/-}$ mice (lower panel) ($n = 4$ mice each) treated with ivermectin (1 mg/kg and 3 mg/kg) or saline over a time course of 5 days. **D** FcγR expressions on resting and IFN-γ-treated splenic macrophages in WT and $Adap^{-/-}$ mice ($n = 4$ mice each) treated with ivermectin for 5 days from (**C**). Splenocytes were either left unstimulated or stimulated with 10 ng/ml IFN-γ for 18 h. F4/80-positive macrophages were gated out and assessed for FcγR expressions. The mean fluorescence intensities of FcγRI and FcγRIV on macrophages in the spleens of WT and $Adap^{-/-}$ mice were determined by flow cytometry (two-way ANOVA, Tukey's multiple comparison). **E** $Adap^{-/-}$ mice that were administrated with anti-mouse GPIbα antibody (R300) at 0.12 mg/kg via s.c. on days 0, 2, and 4 (arrow), were treated with a daily dose of saline, 50 mg/kg fludarabine or 3 mg/kg ivermectin ($n = 6$ mice in each group, two-way ANOVA, Tukey's multiple comparison) starting from day 1. Platelet counts were enumerated over a time course of 6 days. **F** In vitro phagocytosis of DiI-labelled anti-SRBC IgG-opsonized SRBCs by monocyte-derived macrophages from 5 ITP patients in response to IFN-γ and ivermectin (IVM) ($n = 5$, one-way ANOVA, Tukey's multiple comparison). Monocyte-derived macrophages were prepared from circulating monocytes isolated from 5 ITP patients by CD14 positive selection, followed by phagocytosis assay with fluorescence microscopy. A total of approx. 100 cells in each group were analysed. The phagocytic index was calculated as the mean fluorescence intensity multiplied by the percentages of SRBC-phagocytosed macrophages. *$P < 0.05$; **$P < 0.01$; ***$P < 0.001$; ****$P < 0.0001$

binds to importin α and impairs the importin α/β1-mediated nuclear import, and perturbs NLS recognition of virus proteins such as HIV and DENV by importins [63, 64]. It was unknown whether ivermectin could affect NLS recognition and nuclear transport of STAT1 by importin α5. Raw264.7 cells were first primed with increasing doses of ivermectin prior to treatment with IFN-γ for 30 min, and the nuclear translocation of STAT1 and the formation of the STAT1-importin α5 complex were examined. While IFN-γ increased the binding of pY701-STAT1 to importin α5, treatment with ivermectin at low doses (3 and 6 μM) impaired the pY701-STAT1-importin α5 interaction and decreased the nuclear localization of pY701-STAT1 (Fig. 6B). To explore the therapeutic potential of ivermectin for the treatment of thrombocytopenia, we treated WT and $Adap^{-/-}$ mice with ivermectin at daily doses of 1 mg/kg and 3 mg/kg. As shown in Fig. 6C, treatment with ivermectin at 1 mg/kg or 3 mg/kg induced an elevation of platelet counts at day 3 in both WT and $Adap^{-/-}$ mice. Interestingly, when treated with ivermectin at 3 mg/kg, the platelet counts in $Adap^{-/-}$ mice markedly increased to a level comparable to WT mice. In addition, ivermectin treatment downregulated FcγRI and FcγRIV expression in splenic macrophages and decreased the responses of macrophages to IFN-γ stimulation in both WT and $Adap^{-/-}$ mice (Fig. 6D). Moreover, importantly, treatment with a daily dose of ivermectin and fludarabine to inhibit STAT1-importin α5 module mitigated the anti-platelet antibody R300-induced thrombocytopenia in $Adap^{-/-}$ mice at day 6 post dosing(Fig. 6E). Notably, ivermectin treatment also reduced the phagocytic capacity of monocyte-derived macrophages from patients with ITP (Fig. 6F and Supplementary Fig. 4). Collectively, these findings demonstrate that the ADAP-STAT1-importin α5 module is a promising therapeutic target for the treatment of ITP.

DISCUSSION
The link between ADAP and thrombocytopenia was first reported in ADAP gene-knockout mice, showing a 40% reduction in platelet counts relative to WT mice; however the mechanism remained underexplored [25]. Later, Spindler et al. [27] reported that ADAP-deficient mice displayed an intrinsic defect in megakaryocytes, suggesting a role for ADAP in platelet biogenesis. This study explores the role and mechanisms underlying ADAP regulation in the phagocytosis of platelets by macrophages in the context of ITP. To this end, our findings demonstrate that ITP is associated with the underexpression of ADAP in splenic macrophages. ADAP constrains macrophage phagocytic ability by arresting IFN-γ-induced STAT1 nuclear entry, leading to the attenuated transactivation of phagocytosis receptors FcγRI and FcγRIV. Treatment with either a STAT1 inhibitor or an importin α5 inhibitor effectively mitigated thrombocytopenia by decreasing FcγRI and FcγRIV expression in splenic macrophages in $Adap^{-/-}$ mice. Thus, ADAP is central for the homeostatic maintenance of macrophage phagocytosis of platelets.

Macrophage phagocytosis of IgG-opsonized platelet can be prominently regulated by intrinsic changes in FcγRs or FcγR signaling [12, 65, 66]. In addition, extrinsic factors such as C-reactive protein [67], IgG-Fc fucosylation[68], and platelet-bound lipopolysaccharide [69] also modulate macrophage phagocytic capacity. Our study demonstrated an FcγR-intrinsic mechanism for platelet destruction, by which ADAP deficiency selectively enhanced FcγRI/IV-mediated macrophage phagocytosis of platelets, leading to an excessive elimination of platelets. This agrees with a previous report showing that the expression of FcγRI on monocytes was significantly higher in ITP patients, favoring an increased phagocytic capacity [13]. Given that the levels of platelet-associated antibodies were comparable between WT and $Adap^{-/-}$mice, ADAP deficiency possibly sensitizes the macrophage to antibody-opsonized platelets for phagocytosis; this was supported by the evidence that treatment with a very low dose of anti-platelet antibody resulted in a more rapid reduction in platelet counts in $Adap^{-/-}$ mice than in WT mice, and was accompanied by an accelerated clearance of antibody-opsonized platelet. Moreover, RNA-Seq data revealed that a panel of key inflammatory signaling pathways were enriched in $Adap^{-/-}$ splenic macrophages,
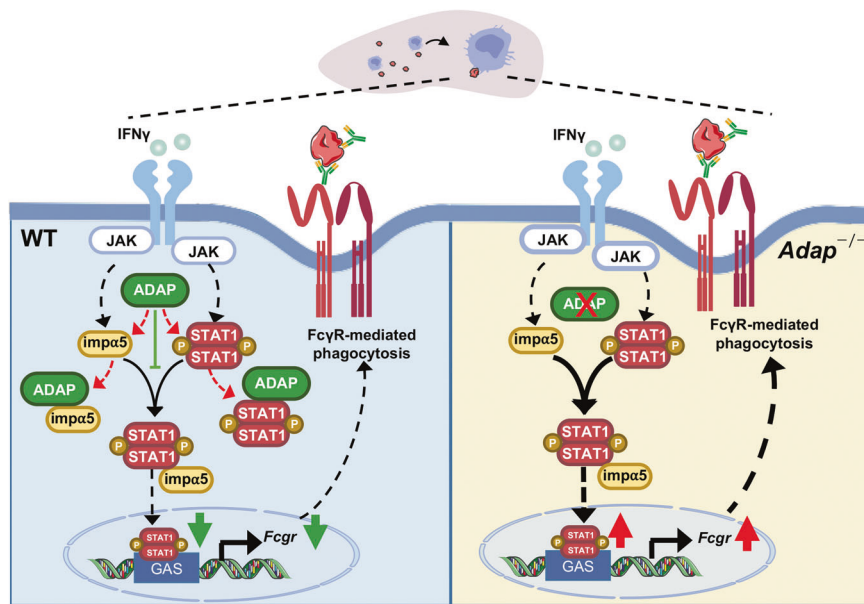
Fig. 7 Schematic model for the selective role of ADAP in macrophage-mediated platelet phagocytosis by targeting the STAT1-importin α5-FcγR axis. ADAP interacts and competes with STAT1 binding to importin α5 to keep a portion of IFN-γ-activated STAT1 anchored in the cytosol so that the activation of macrophages is maintained within a desired physiological range. This restraint is removed when ADAP is underexpressed in macrophages, leading to an enhancement of STAT1-dependent transactivation of FcγRI and FcγRIV. As such, the heightened phagocytic ability of macrophages is induced, causing excessive phagocytic clearance of platelets and contributing to ITP pathogenesis

including the NLR signaling and IL-23/IL-17 pathways, as well as IFN production, suggesting that ADAP deficiency skews macrophage activation toward a proinflammatory phenotype. This is consistent with the prevalence of a proinflammatory macrophage phenotype in the spleen of ITP patients [70]. Thus, these combined effects of heightened FcγR-mediated platelet destruction with increased inflammatory signaling in $Adap^{-/-}$ macrophages aggravate the development of thrombocytopenia. In supporting this notion, a recent study suggested that an anti-inflammatory antibody, anti-CD44, ameliorates ITP by inhibiting macrophage FcγR-mediated phagocytosis of platelets after its Fc fragment blocking FcγR IgG binding site (the Kurlander phenomenon) [71, 72].

Mechanistically, we showed that ADAP interacts and competes with STAT1 for binding to importin α5, a nuclear import carrier of STAT1 (Fig. 7). Thus, ADAP functions as a cytoplasmic anchor or an in-built phagocytosis checkpoint for STAT1 nuclear entry in macrophages. As such, the level of IFN-γ-STAT1-induced and FcγR-dependent phagocytosis by macrophages is maintained within a desired physiologic range. Interestingly, similar examples were seen with SARS-CoV-2 Orf6 protein, which impairs docking of importins at the nuclear pore complex to disrupt STAT1 nuclear import [73], and with Ebola virus VP24, which selectively targets importin α5 and competes with nuclear import of phosphorylated STAT1 [74]. We reasoned targeting the ADAP-STAT1-importin α5 module would ameliorate thrombocytopenia. Indeed, our in vivo data indicate that treatment with the importin α5 inhibitor ivermectin effectively abrogates STAT1-importin α5 interactions and, more importantly, mitigates the phenotype of thrombocytopenia by decreasing FcγRI and FcγRIV expression in $Adap^{-/-}$ mice. Moreover, as expected, inhibition of STAT1 by fludarabine obtained a similar effect in $Adap^{-/-}$ mice, where the low platelet counts were reversed. Notably, the phagocytic capacity of monocyte-derived macrophages from patients with ITP were substantially reduced after priming with ivermectin. Therefore, the ADAP-STAT1-importin α5 module can be targeted for therapeutic intervention against ITP.

Together, our findings suggest a novel mechanism in the regulation of platelet destruction, whereby ADAP restrains platelet phagocytosis by macrophages through competing with STAT1 binding to importin α5. Our work not only sheds new light on the pathogenesis of ITP but also provides a promising strategy for therapeutic intervention in the treatment of ITP.

DATA AVAILABILITY
RNA-seq data have been deposited in the GEO database under accession number GSE183385. All related data, code, and materials used in the analyses are available from the corresponding author (Dr. Hebin Liu, hbliu@suda.edu.cn) upon reasonable request.

REFERENCES
1. Rodeghiero F, Stasi R, Gernsheimer T, Michel M, Provan D, Arnold DM, et al. Standardization of terminology, definitions and outcome criteria in immune thrombocytopenic purpura of adults and children: report from an international working group. Blood 2009;113:2386–93.
2. Cooper N, Ghanima W. Immune Thrombocytopenia. N Engl J Med. 2019;381:945–55.
3. Terrell DR, Beebe LA, Vesely SK, Neas BR, Segal JB, George JN. The incidence of immune thrombocytopenic purpura in children and adults: A critical review of published reports. Am J Hematol. 2010;85:174–80.
4. Swinkels M, Rijkers M, Voorberg J, Vidarsson G, Leebeek FWG, Jansen AJG. Emerging concepts in immune thrombocytopenia. Front Immunol. 2018;9:880.
5. Cines DB, Bussel JB, Liebman HA, Luning, Prak ET. The ITP syndrome: Pathogenic and clinical diversity. Blood 2009;113:6511–21.
6. Guan WJ, Ni ZY, Hu Y, Liang WH, Ou CQ, He JX, et al. Clinical characteristics of coronavirus disease 2019 in China. N Engl J Med. 2020;382:1708–20.
7. Porcelijn L, Huiskes E, Oldert G, Schipperus M, Zwaginga JJ, de Haas M. Detection of platelet autoantibodies to identify immune thrombocytopenia: state of the art. Br J Haematol. 2018;182:423–6.
8. Zufferey A, Kapur R, Semple JW. Pathogenesis and Therapeutic Mechanisms in Immune Thrombocytopenia (ITP). J Clin Med. 2017;6. https://doi.org/10.3390/jcm6020016.
9. Crow AR, Lazarus AH. Role of Fcgamma receptors in the pathogenesis and treatment of idiopathic thrombocytopenic purpura. J Pediatr Hematol Oncol. 2003;25:S14–18.
10. Norris PAA, Segel GB, Burack WR, Sachs UJ, Lissenberg-Thunnissen SN, Vidarsson G, et al. FcgammaRI and FcgammaRIII on splenic macrophages mediate phagocytosis of anti-glycoprotein IIb/IIIa autoantibody-opsonized platelets in immune thrombocytopenia. Haematologica 2021;106:250–4.
11. Bruhns P. Properties of mouse and human IgG receptors and their contribution to disease models. Blood 2012;119:5640–9.
12. Nimmerjahn F, Ravetch JV. Fcgamma receptors as regulators of immune responses. Nat Rev Immunol. 2008;8:34–47.
13. Liu X-G, Ma S-H, Sun J-Z, Ren J, Shi Y, Sun L, et al. High-dose dexamethasone shifts the balance of stimulatory and inhibitory Fcγ receptors on monocytes in patients with primary immune thrombocytopenia. Blood 2011;117:2061–9.
14. Olsson B, Andersson PO, Jernas M, Jacobsson S, Carlsson B, Carlsson LM, et al. T-cell-mediated cytotoxicity toward platelets in chronic idiopathic thrombocytopenic purpura. Nat Med. 2003;9:1123–4.
15. Qiu J, Liu X, Li X, Zhang X, Han P, Zhou H, et al. CD8(+) T cells induce platelet clearance in the liver via platelet desialylation in immune thrombocytopenia. Sci Rep. 2016;6:27445.
16. Panitsas FP, Theodoropoulou M, Kouraklis A, Karakantza M, Theodorou GL, Zoumbos NC, et al. Adult chronic idiopathic thrombocytopenic purpura (ITP) is the manifestation of A type-1 polarized immune response. Blood 2004;103:2645–7.
17. Semple JW, Milev Y, Cosgrave D, Mody M, Hornstein A, Blanchette V, et al. Differences in serum cytokine levels in acute and chronic autoimmune thrombocytopenic purpura: relationship to platelet phenotype and antiplatelet T-cell reactivity. Blood 1996;87:4245–54.
18. Stark GR, Darnell JE Jr. The JAK-STAT pathway at twenty. Immunity 2012;36:503–14.
19. Ramana CV, Chatterjee-Kishore M, Nguyen H, Stark GR. Complex roles of Stat1 in regulating gene expression. Oncogene 2000;19:2619–27.
20. Sekimoto T, Imamoto N, Nakajima K, Hirano T, Yoneda Y. Extracellular signal-dependent nuclear import of Stat1 is mediated by nuclear pore-targeting complex formation with NPI-1, but not Rch1. EMBO J. 1997;16:7067–77.
21. Fagerlund R, Melen K, Kinnunen L, Julkunen I. Arginine/lysine-rich nuclear localization signals mediate interactions between dimeric STATs and importin alpha 5. J Biol Chem. 2002;277:30072–8.
22. Chen Z, Guo Z, Ma J, Liu F, Gao C, Liu S, et al. STAT1 single nucleotide polymorphisms and susceptibility to immune thrombocytopenia. Autoimmunity 2015;48:305–12.
23. Liu D, Epstein I. A Rare Cause of Non Cirrhotic Variceal Bleeding: Stat1 Gene Mutation and ITP: 1835. Off J American College Gastroenterol. 2016;111:S880–1.
24. Jarvis GE, Bihan D, Hamaia S, Pugh N, Ghevaert CJ, Pearce AC, et al. A role for adhesion and degranulation-promoting adapter protein in collagen-induced platelet activation mediated via integrin alpha(2) beta(1). J Thromb Haemost. 2012;10:268–77.
25. Peterson EJ, Woods ML, Dmowski SA, Derimanov G, Jordan MS, Wu JN, et al. Coupling of the TCR to integrin activation by Slap-130/Fyb. Science 2001;293:2263–5.
26. Kasirer-Friede A, Moran B, Nagrampa-Orje J, Swanson K, Ruggeri ZM, Schraven B, et al. ADAP is required for normal alphaIIbbeta3 activation by VWF/GP Ib-IX-V and other agonists. Blood 2007;109:1018–25.
27. Spindler M, van Eeuwijk JMM, Schurr Y, Nurden P, Nieswandt B, Stegner D, et al. ADAP deficiency impairs megakaryocyte polarization with ectopic proplatelet release and causes microthrombocytopenia. Blood 2018;132:635–46.
28. Hamamy H, Makrythanasis P, Al-Allawi N, Muhsin AA, Antonarakis SE. Recessive thrombocytopenia likely due to a homozygous pathogenic variant in the FYB gene: Case report. BMC Med Genet. 2014;15:135.
29. Levin C, Koren A, Pretorius E, Rosenberg N, Shenkman B, Hauschner H, et al. Deleterious mutation in the FYB gene is associated with congenital autosomal recessive small-platelet thrombocytopenia. J Thromb Haemost. 2015;13:1285–92.
30. Wang H, Liu H, Lu Y, Lovatt M, Wei B, Rudd CE. Functional defects of SKAP-55-deficient T cells identify a regulatory role for the adaptor in LFA-1 adhesion. Mol Cell Biol. 2007;27:6863–75.
31. Fujiyama S, Nakahashi-Oda C, Abe F, Wang Y, Sato K, Shibuya A. Identification and isolation of splenic tissue-resident macrophage sub-populations by flow cytometry. Int Immunol. 2019;31:51–56.

32. Yang NQ, Xiong YW, Wang Y, Yi YL, Zhu JF, Ma F, et al. ADAP Y571 Phosphorylation Is Required to Prime STAT3 for Activation in TLR4-Stimulated Macrophages. J Immunol. 2021;206:814–26.

33. Liu XG, Liu S, Feng Q, Liu XN, Li GS, Sheng Z, et al. Thrombopoietin receptor agonists shift the balance of Fcgamma receptors toward inhibitory receptor IIb on monocytes in ITP. Blood 2016;128:852–61.

34. Crow AR, Song S, Semple JW, Freedman J, Lazarus AH. IVIg inhibits reticuloendothelial system function and ameliorates murine passive-immune thrombocytopenia independent of anti-idiotype reactivity. Br J Haematol. 2001;115:679–86.

35. Jaumouille V, Cartagena-Rivera AX, Waterman CM. Coupling of beta2 integrins to actin by a mechanosensitive molecular clutch drives complement receptor-mediated phagocytosis. Nat Cell Biol. 2019;21:1357–69.

36. Bezbradica JS, Rosenstein RK, DeMarco RA, Brodsky I, Medzhitov R. A role for the ITAM signaling module in specifying cytokine-receptor functions. Nat Immunol. 2014;15:333–42.

37. Fitzer-Attas CJ, Lowry M, Crowley MT, Finn AJ, Meng F, DeFranco AL, et al. Fcgamma receptor-mediated phagocytosis in macrophages lacking the Src family tyrosine kinases Hck, Fgr, and Lyn. J Exp Med. 2000;191:669–82.

38. Xiong Y, Ye C, Yang N, Li M, Liu H. Ubc9 Binds to ADAP and Is Required for Rap1 Membrane Recruitment, Rac1 Activation, and Integrin-Mediated T Cell Adhesion. J Immunol. 2017;199:4142–54.

39. Aittomaki S, Yang J, Scott EW, Simon MC, Silvennoinen O. Distinct functions for signal transducer and activator of transcription 1 and PU.1 in transcriptional activation of Fc gamma receptor I promoter. Blood 2002;100:1078–80.

40. Doench JG, Fusi N, Sullender M, Hegde M, Vaimberg EW, Donovan KF, et al. Optimized sgRNA design to maximize activity and minimize off-target effects of CRISPR-Cas9. Nat Biotechnol. 2016;34:184–91.

41. Sanjana NE, Shalem O, Zhang F. Improved vectors and genome-wide libraries for CRISPR screening. Nat Methods. 2014;11:783–4.

42. Shen H, Campanello GC, Flicker D, Grabarek Z, Hu J, Luo C, et al. The human knockout gene CLYBL connects itaconate to Vitamin B12. Cell 2017;171:771–82 e711.

43. Xiong Y, Yi Y, Wang Y, Yang N, Rudd CE, Liu H. Ubc9 Interacts with and SUMOylates the TCR Adaptor SLP-76 for NFAT Transcription in T Cells. J Immunol. 2019;203:3023–36.

44. Yu Z, Huang Z, Lung ML. Subcellular fractionation of cultured human cell lines. Bio-Protoc. 2013;3:e754.

45. Sotillo E, Garriga J, Padgaonkar A, Kurimchak A, Cook JG, Graña X. Coordinated activation of the origin licensing factor CDC6 and CDK2 in resting human fibroblasts expressing SV40 small T antigen and cyclin E. J Biol Chem. 2009;284:14126–35.

46. Singh B, Nath SK. Identification of Proteins Interacting with Single Nucleotide Polymorphisms (SNPs) by DNA Pull-Down Assay. In: Kurien BT, Scofield RH (eds). Electrophoretic Separation of Proteins: Methods and Protocols. Springer New York: New York, NY, 2019, pp 355–62.

47. Jernas M, Hou Y, Stromberg Celind F, Shao L, Nookaew I, Wang Q, et al. Differences in gene expression and cytokine levels between newly diagnosed and chronic pediatric ITP. Blood 2013;122:1789–92.

48. Jernas M, Nookaew I, Wadenvik H, Olsson B. MicroRNA regulate immunological pathways in T-cells in immune thrombocytopenia (ITP). Blood 2013;121:2095–8.

49. Jernas M, Stromberg Celind F, Nookaew I, Mellgren K, Wadenvik H, Olsson B. Normalised immune expression in remission of paediatric ITP. Thromb Haemost. 2016;115:1229–30.

50. Ritchie ME, Phipson B, Wu D, Hu Y, Law CW, Shi W, et al. limma powers differential expression analyses for RNA-sequencing and microarray studies. Nucleic Acids Res. 2015;43:e47.

51. Liu J, Kang H, Raab M, da Silva AJ, Kraeft SK, Rudd, et al. FYB (FYN binding protein) serves as a binding partner for lymphoid protein and FYN kinase substrate SKAP55 and a SKAP55-related protein in T cells. Proc Natl Acad Sci USA. 1998;95:8779–84.

52. Morodomi Y, Kanaji S, Won E, Ruggeri ZM, Kanaji T. Mechanisms of anti-GPIbalpha antibody-induced thrombocytopenia in mice. Blood 2020;135:2292–301.

53. Gordon S. Phagocytosis: An immunobiologic process. Immunity 2016;44:463–75.

54. Lee TY, Chang WC, Hsu JB, Chang TH, Shien DM. GPMiner: An integrated system for mining combinatorial cis-regulatory elements in mammalian gene group. BMC Genomics. 2012;13:S3.

55. da Silva AJ, Li Z, de Vera C, Canto E, Findell P, Rudd CE. Cloning of a novel T-cell protein FYB that binds FYN and SH2-domain-containing leukocyte protein 76 and modulates interleukin 2 production. Proc Natl Acad Sci USA. 1997;94:7493–8.

56. Musci MA, Hendricks-Taylor LR, Motto DG, Paskind M, Kamens J, Turck CW, et al. Molecular cloning of SLAP-130, an SLP-76-associated substrate of the T cell antigen receptor-stimulated protein tyrosine kinases. J Biol Chem. 1997;272:11674–7.

57. Robbins J, Dilworth SM, Laskey RA, Dingwall C. Two interdependent basic domains in nucleoplasmin nuclear targeting sequence: Identification of a class of bipartite nuclear targeting sequence. Cell 1991;64:615–23.

58. McBride KM, Banninger G, McDonald C, Reich NC. Regulated nuclear import of the STAT1 transcription factor by direct binding of importin-alpha. EMBO J. 2002;21:1754–63.

59. Melen K, Kinnunen L, Julkunen I. Arginine/lysine-rich structural element is involved in interferon-induced nuclear import of STATs. J Biol Chem. 2001;276:16447–55.

60. Melen K, Fagerlund R, Franke J, Kohler M, Kinnunen L, Julkunen I. Importin alpha nuclear localization signal binding sites for STAT1, STAT2, and influenza A virus nucleoprotein. J Biol Chem. 2003;278:28193–28200.

61. Frank DA, Mahajan S, Ritz J. Fludarabine-induced immunosuppression is associated with inhibition of STAT1 signaling. Nat Med. 1999;5:444–7.

62. Chen IS, Kubo Y. Ivermectin and its target molecules: shared and unique modulation mechanisms of ion channels and receptors by ivermectin. J Physiol. 2018;596:1833–45.

63. Wagstaff KM, Sivakumaran H, Heaton SM, Harrich D, Jans DA. Ivermectin is a specific inhibitor of importin α/β-mediated nuclear import able to inhibit replication of HIV-1 and dengue virus. Biochemical J. 2012;443:851–6.

64. Yang SNY, Atkinson SC, Wang C, Lee A, Bogoyevitch MA, Borg NA, et al. The broad spectrum antiviral ivermectin targets the host nuclear transport importin alpha/beta1 heterodimer. Antivir Res. 2020;177:104760.

65. Samuelsson A, Towers TL, Ravetch JV. Anti-inflammatory activity of IVIG mediated through the inhibitory Fc receptor. Science 2001;291:484–6.

66. Podolanczuk A, Lazarus AH, Crow AR, Grossbard E, Bussel JB. Of mice and men: an open-label pilot study for treatment of immune thrombocytopenic purpura by an inhibitor of Syk. Blood 2009;113:3154–60.

67. Kapur R, Heitink-Polle KM, Porcelijn L, Bentlage AE, Bruin MC, Visser R, et al. C-reactive protein enhances IgG-mediated phagocyte responses and thrombocytopenia. Blood 2015;125:1793–802.

68. Kapur R, Kustiawan I, Vestrheim A, Koeleman CA, Visser R, Einarsdottir HK, et al. A prominent lack of IgG1-Fc fucosylation of platelet alloantibodies in pregnancy. Blood 2014;123:471–80.

69. Semple JW, Aslam R, Kim M, Speck ER, Freedman J. Platelet-bound lipopolysaccharide enhances Fc receptor-mediated phagocytosis of IgG-opsonized platelets. Blood 2007;109:4803–5.

70. Feng Q, Xu M, Yu YY, Hou Y, Mi X, Sun YX, et al. High-dose dexamethasone or all-trans-retinoic acid restores the balance of macrophages towards M2 in immune thrombocytopenia. J Thromb Haemost. 2017;15:1845–58.

71. Norris PAA, Kaur G, Khan R, Zhu G, Ni H, Lazarus AH. Anti-inflammatory activity of CD44 antibodies in murine immune thrombocytopenia is mediated by Fcgamma receptor inhibition. Blood 2021;137:2114–24.

72. Kurlander RJ. Blockade of Fc receptor-mediated binding to U-937 cells by murine monoclonal antibodies directed against a variety of surface antigens. J Immunol. 1983;131:140–7.

73. Miorin L, Kehrer T, Sanchez-Aparicio MT, Zhang K, Cohen P, Patel RS, et al. SARS-CoV-2 Orf6 hijacks Nup98 to block STAT nuclear import and antagonize interferon signaling. Proc Natl Acad Sci USA. 2020;117:28344–54.

74. Xu W, Edwards MR, Borek DM, Feagins AR, Mittal A, Alinger JB, et al. Ebola virus VP24 targets a unique NLS binding site on karyopherin alpha 5 to selectively compete with nuclear import of phosphorylated STAT1. Cell Host Microbe. 2014;16:187–200.

AUTHOR CONTRIBUTIONS

H.L. and Y.X. conceived the study; Y.X. and H.L. designed experiments; Y.X., Y.L., and X.C. performed experiments; Y.X., L.Z., and H.L. analyzed and interpreted data; L.Z. and X.Y. performed pathologic examination and provided patient tissue samples; Y.X. and H.L. wrote and edited the manuscript with intellectual input from the other authors; H.L. supervised and acquired funding for the study.

COMPETING INTERESTS

The authors declare no competing interests.

ADDITIONAL INFORMATION

Supplementary information The online version contains supplementary material available at https://doi.org/10.1038/s41423-022-00881-2.

Correspondence and requests for materials should be addressed to Hebin Liu.

Reprints and permission information is available at http://www.nature.com/reprints